Journal of Medical Imaging

Journal of Medical Imaging

Journal of Medical Imaging

OPEN ACCESS

Analysis of the DWT Characteristics of MR Molecular Images Obtained by Using MNPCA

Junhaeng Lee Ph.D

Abstract- I was suggested a method to analyze the DWT(discrete wavelet transform) characteristics of magnetic resonance(MR) molecular images obtained by using contrast agent made of magnetic nanoparticles. The magnetic nanoparticles contrast agents(MNCA) were prepared by thermal decomposition method. We transplanted gastric cancer stem cells into experimental mice four weeks before the experiment. After injecting MNCA into the prepared mice, the MR molecule images were obtained as follows: before to MNCA injection, immediately after MNCA injection, 2 hours after MNCA injection and 4 hours after MNCA injection. At this time, we were used pulse sequence which T_2 TSE, T_2 MPGR, T_2^*, and UTE. We extracted and analyzed the signal characteristics of the pulse sequence of MR molecular images obtained by MNCA. The characteristics between T_2 signal (T_2 MPGR, T_2 TSE, T_2^*) and UTE (Ultra short TE) were extracted and compared. Feature extraction for each signal was performed by the DWT method. The M program for DWT 3-step decomposition was used the MATLAB Toolbox. After decomposing in 3-step, we extracted the horizontal low frequency (A4H), vertical low frequency (A4V), horizontal high frequency (H4V), vertical high frequency (V4H), horizontal diagonal high frequency (D4H) and high frequency (D4V).

Junhaeng Lee ✉ *corresponding author*

(62271)Deptartment of Radiology, Nambu University

23, Chumdan Jungang-ro, Gwangsan-gu, Gwangju,

Korea

The extracted features were compared and analyzed for each pulse signals. The results of this study can be used to demonstrate the effectiveness of MNCA for the usefulness of MR molecular imaging and UTE signals.

I.   Introduction

Nowadays, medical scientists have been clearly analyzed to diagnose of disease through change of in molecular level which of fundamental stages of disease, it is effort to develop the nano medical technology for predict outcomes of disease treatment. The age of precision medicine is approaching with the convergence of medical science and nanotechnology, precision medicine is a technology that enables to diagnosis and treat using bio compatible nano-bio chip, nano robot, and so on. Nanotechnology has also been applied to the field of medical imaging, enabling to the acquisition of molecular imaging. Molecular imaging is enable to

ScholarGen

early diagnosis for recognizing changes in the cellular level prior to developing of disease, also, it is can predict the prognosis after treatment [1-3]. Positron emission tomography (PET), Magnetic resonance imaging (MRI), and Computed tomography (CT) are widely used as imaging modality for molecular imaging. Among these imaging modality, PET has excellent sensitivity and specificity, but it has disadvantages of using radioisotope and low spatial resolution and tissue contrast [4-5]. MRI devices have the advantage of acquiring images with high resolution and tissue contrast without using ionizing radiation [6-13]. However, it has disadvantage that acquisition process of the signal is relatively longer than Computed tomography. The development of nanotechnology for MR molecular imaging is active in the field of nano contrast agent. In this study, we propose a novel imaging method through conventional T2 weighted imaging (T2W), Ultra short TE (UTE) using a nano contrast agents. The features are extracted and compared to between conventional T2 (T2 MPGR, T2 TSE, T2 STAR) and Ultra short TE (UTE) for evaluate the efficiency of the proposed UTE pulse sequence. Feature extraction is performed by the DWT (Discrete wavelet transform) method, it is a method of decomposing a signal into a set of base functions such as Fourier transform. The program for the DWT three-step decomposition was used in the MATLAB Tool Box. After decomposing in three steps, the feature of the components of horizontal low frequency (A4H), vertical low frequency (A4V), horizontal high frequency (H4V), vertical high frequency (V4H), horizontal diagonal high frequency (D4H), vertical diagonal high frequency (D4V) in the low frequency region were extracted. The results of this study can be used to demonstrate the efficiency of the nano-contrast agent for MR imaging and the utility of the UTE signal.

II. Materials and Methods

A. Materials

Polysorbate 80 (P80), ethylenediamine, 1,4-dioxane (99.8%), and 1,1'-carbonyldiimidazole (CDI) were purchased from Sigma Aldrich Chemical Co. Phosphate buffered saline (PBS: 10 mM, pH 7.4), Roswell Park Memorial Institute-1640 (RPMI-1640), fetal bovine serum (FBS) and antibiotic-antimycotic solution were purchased from Gibco and dialysis membrane (1 kDa MWCO) from Spectrum laboratory. Hyaluronic acid (1 MDa) was supplied from Yuhan Phrmaceutical Corporation (Seoul, Korea). MKN-45 (American Tissue Type Culture) cell line was grown in medium containing 10% FBS and 1% antibiotic antimycotic at 37°C and a humidified 5% CO_2 atmosphere. Ultrapure deionized water was used for all of the syntheses.

B. Methods

1. Synthesis of magnetic nanoparticles contrast agent

The magnetic nanoparticles contrast agents (MNCA) were prepared by thermal decomposition method. Briefly, 2 mmol iron (III) acetylacetonate, 1 mmol manganese (II) acetylacetonate, 10 mmol 1,2-hexadecanediol, 6 mmol dodecanoic acid, and 6 mmol dodecylamine were dissolved in 20 mL benzyl ether under an ambient nitrogen atmosphere. The mixture was then preheated to 200 °C for 2 h and refluxed at 300 °C for 30 min. After the reactants were cooled to room temperature, the products were purified with an excess of pure ethanol. Approximately 11 nm MNCAs were synthesized using the seed-mediated growth method.

2. Feature Extraction on Image by DWT

The Discrete Wavelet Transform (DWT) is converted the signal from the spatial domain to the frequency domain. The human eye is more sensitive to the information of the low frequency component than the high frequency component [15]. Thus, DWT is used for JPEG compression algorithms, boundary detection, and to extract texture information from an image. It is also used for contour extraction by using the conversion coefficients of low frequency and medium frequency components most sensitive to contour information among DWT coefficients [16]. In order to solve the disadvantage of STFT's fixed resolution, wavelet transform is performed by applying a short window to the high-frequency band in the time-frequency plane to increase the temporal resolution, In the low-frequency range, the frequency resolution can be increased by applying a long window [17-19]. The wavelet transform introduced by ingrid Daubechies and Stephane Mallat is a method of decomposing the signal into a set of basis functions such as Fourier transform [17]. However, unlike Fourier transform, wavelets, which are band-pass signals with local energy concentration, are used as basis functions. These wavelets can be obtained by extending and moving a single prototype wavelet called a mother wavelet. The wavelet transform refers to an expansion factor that is several times larger than the frequency of the extended signal, and this factor is called the scale. At this time, a value of scale is mainly used as a multiple of 2^n [20]. As the scale increases, the spatial resolution of the wavelet transform signal is decreases at a given scale and appear the low frequency components [20]. The

wavelet transform is obtained to $\Psi(\varkappa)$ by dilating / translating the circular wavelet in Equation. (1) [19].

$$\Psi_{\alpha,\beta}(\varkappa) = \frac{1}{\sqrt{\alpha}} \Psi\left(\frac{\varkappa-\delta}{\alpha}\right)$$

(Equation 1)

Herein, α is scaling coefficient, β is translation coefficient. And $\alpha^{1/2}$ is normalization factor, if $\alpha < 1$, high-frequency wavelet having a small width on the time axis, if $\alpha > 1$, it is a wide-frequency wavelet. The shape of the wavelet varies according to the proposed person, Application areas differ depending on the characteristics and advantages of each wavelet. The two-dimensional signal decomposed on an orthonormal basis is decomposed into spatially directional frequency components as shown in Equation. (2) [19].

$$\begin{aligned}
A_{2^{m+1}}f &= \sum_k \sum_l h(2m-k)\,h(2n-l)\,A_{2^j}f \\
H_{2^{m+1}}f &= \sum_k \sum_l h(2m-k)\,g(2n-l)\,A_{2^j}f \\
V_{2^{m+1}}f &= \sum_k \sum_l g(2m-k)\,h(2n-l)\,A_{2^j}f \\
D_{2^{m+1}}f &= \sum_k \sum_l g(2m-k)\,g(2n-l)\,A_{2^j}f
\end{aligned}$$

(Equation 2)

In equation (2), h is transfer function of the decomposition low pass filter, g is transfer function of the decomposition high pass filter. [Figure. 2] showed decomposition and synthesis of two-dimensional signals by DWT, [Figure. 2] (a) is the decomposition process of the 2-D discrete approximate signal and [Figure. 2] (b) is a block diagram of the synthesis process. [Figure. 2] (c) shows the coefficient matrix of the two-dimensional signal decomposed into multiple resolutions, That is, a coefficient matrix that is two-level decomposed into packets of frequency component having spatial directionality, [Figure. 2] (c), VH1 means a coefficient matrix of vertical high-frequency components decomposed at level 1, HH1 and DH1 mean the coefficient matrix of the horizontal high-

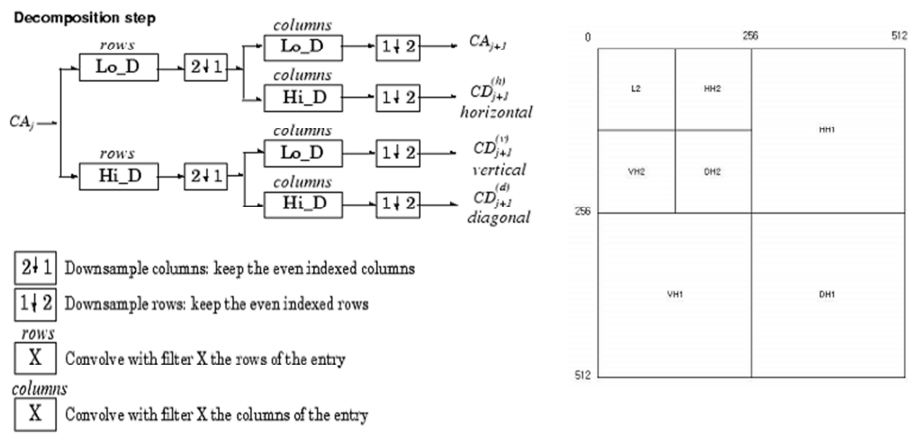frequency component and the diagonal high-   frequency component, respectively.

Figure 2. Decomposition and synthesis of two-dimensional signals by DWT

III.   Experiments and results

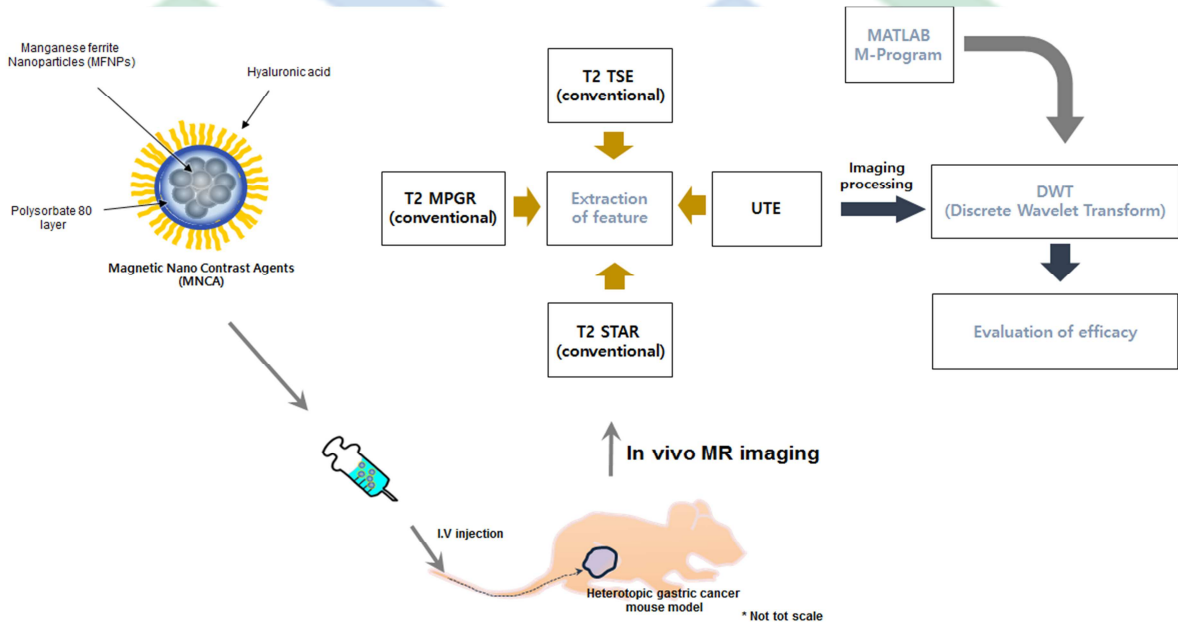### A. Schematic illustration

Figure 3. Preparing the experimental model

As shown in figure 3, the experiment was designed and proceeded after injecting the synthesized contrast agent into the body of a mouse. The obtained MR images (T2 TSE, T2 MPGR, T2 STAR, UTE) were compared and analyzed by the proposed image technique in this paper.

B. Acquisition of MR Molecular Imaging

All animal studies were approved and accredited by the Association for Assessment and Accreditation of Laboratory Animal Care (AAALAC) International.

Six-week-old female nude mice were injected intravenously with an anesthetic Zoletil / Rompun mixture. After anesthesia, the mice were injected to 1.0×10^7 gastric cancer cells which after dispersing in 200 mL of saline solution into thighs. And then, MR imaging were obtained on the 5th week after transplanting the gastric cancer cell line. MR imaging was performed with 3 T SIMENS clinical instruments using a wrist coil. Imaging was performed as follows: Pre-contrast, Immediate (IMM), 2 h after (2H), and 4 h after (4 h) imaging as shown table 2. (Table 1 : MR parameter, Figure. 4 : pulse diagram)
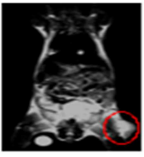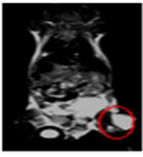
Table -1. Sequence (3T SIEMENS)
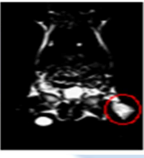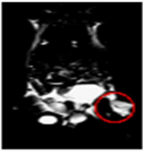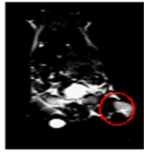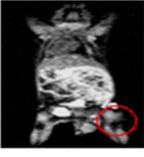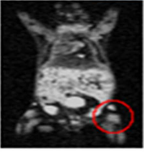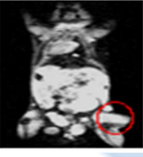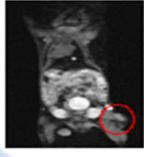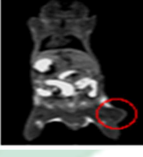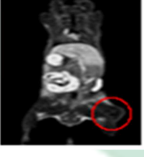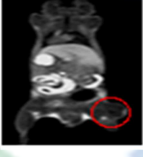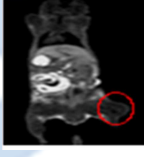
	FOV read	FOV phase	Slice Thickness	TR	TE
T2 MPGR	100 mm	87.5 %	1.50 mm	594 ms	15.0 ms
T2 TSE	100 mm	80.4 %	1.00 mm	4140 ms	113 ms
T2 STAR	100 mm	100 %	1.00 mm	14.85 ms	5.85 ms
UTE	110 mm	100 %	0.57 mm	6.72 ms	0.07 ms
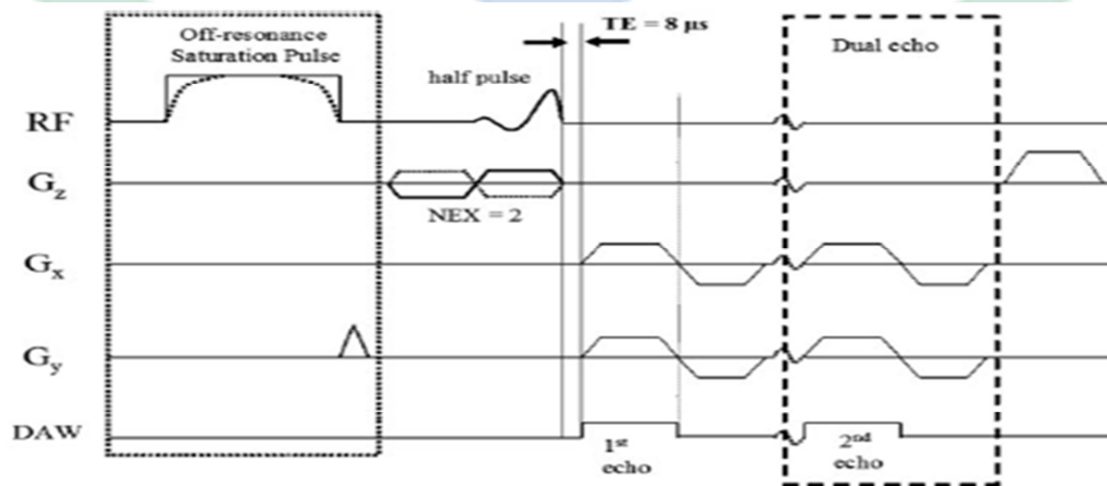
Figure 4. Pulse sequence

Table-2. Molecular MR Imaging of CD44-expressed Gastric Cancer in Mice using T2 and Ultra Short TE Pulse Sequences

	Pre	IMM	After 2H	Afetr 4H
T2 MPGR MRI				
T2 TSE MRI				
T2 star MRI				
UTE MRI				

C. Feature Extraction

The region of the stomach cancer cells in the acquired image was set as the region of interest (ROI). The separated images were adjusted in the form of 256 x 256 pixels for the same experiment with MATLAB Tool Box, the number of bits per pixel was adjusted to 8 bits. The experimental procedure was performed in the order of Figure 5.

Table 3. Feature parameters of coefficient matrix.

Abbreviation	Meaning of feature extraction parameter
A4H	low frequency coefficient matrix (horizontal direction)
A4V	low frequency coefficient matrix (vertical direction)
H4V	horizontal high-frequency coefficient matrix
V4H	vertical high-frequency coefficient matrix
D4H	diagonal high frequency coefficient matrix (horizontal direction)
D4V	diagonal high frequency coefficient matrix (vertical direction)
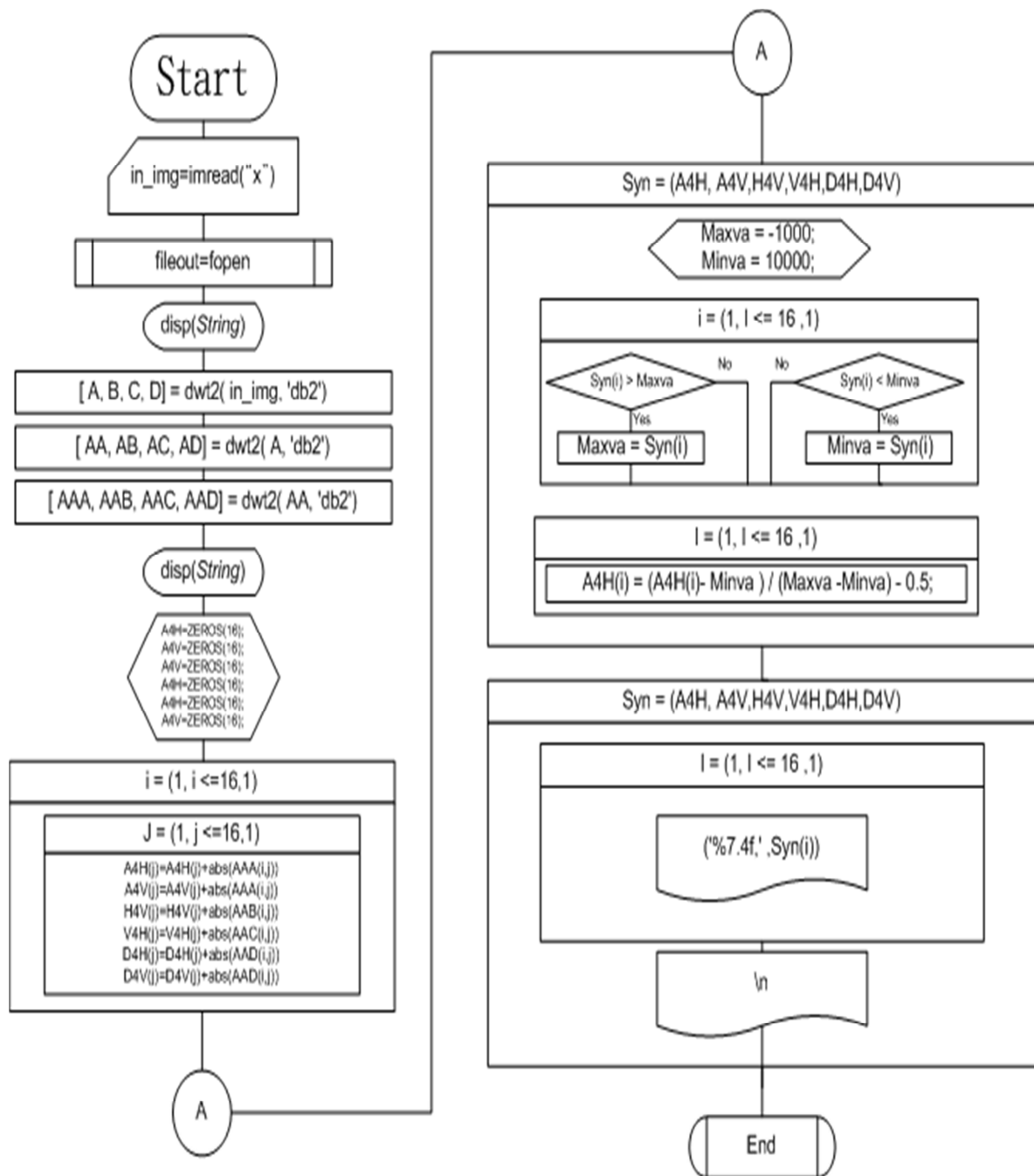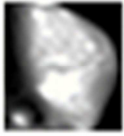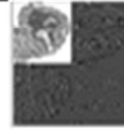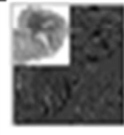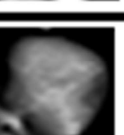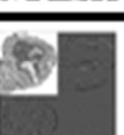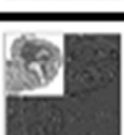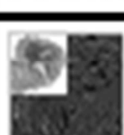
Figure 5. Feature Extraction Flow chart

D. Results of DWT
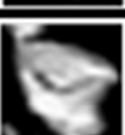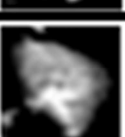
The results of the T2 MPGR MR image, the T2 TSE

MR image, the T2 star MR image, and the UTE image DWT obtained by the program execution are shown in Table 5.
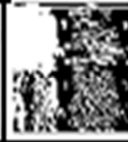
Table-4. DWT results of T2 MPGR MRI
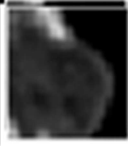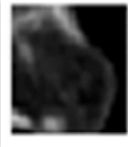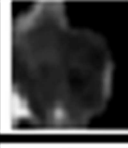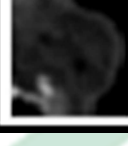
Table-5. DWT results of T2 TSE MRI

Table-6. DWT results of T2 star MRI

		ROI	DWT		
		Image	1 Level	2 Level	3 Level
T2 star MR image	Pre				
	IMM				
	2H				
	4H				

Table-7. DWT results of UTE MRI

		ROI	DWT		
		Image	1 Level	2 Level	3 Level
UTE	Pre				
MR image	IMM				
	2H				
	4H				

IV. Conclusion and discussion

Nanotechnology using magnetic resonance imaging (MRI) devices has led to active development of nano-contrast agents. The aim of this study was to evaluate the usefulness of T2 signals and UTE signals in molecular MR images obtained after injection of nanoparticle agents into mice which of gastric cancer expressing CD44.

A. Pre-Injection

T2 pulse sequence and UTE signal before injection of contrast agent showed similar frequency change in horizontal low frequency signal, vertical low frequency signals showed only different UTE signals. Horizontal high frequency, vertical high frequency, and diagonal high frequency were high frequency
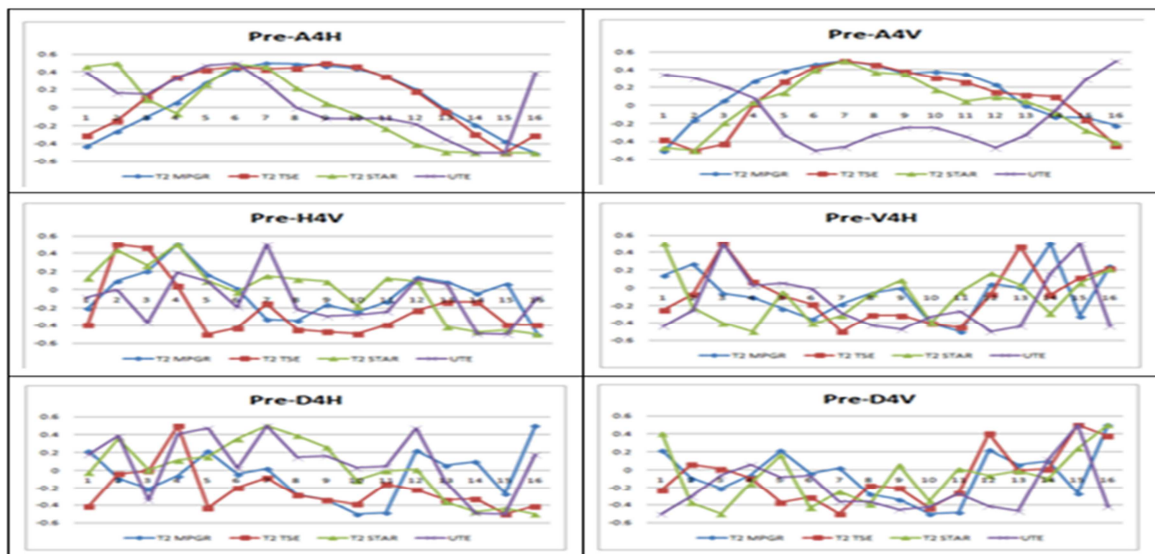
Figure 6. Analysis of signal in low frequency region after 3 Level DWT before contrast agent Injection.

B. Injection Immediately

Immediately after injecting the contrast agent, the T2 pulse sequence and the UTE signal showed similar frequency changes in the horizontal low frequency signals, vertical low frequency signals are different from UTE signal and T2 MPGR image only. The horizontal high - frequency component showed no change only in T2 MPGR component, vertical high frequency, each diagonal high frequency showed high frequency.
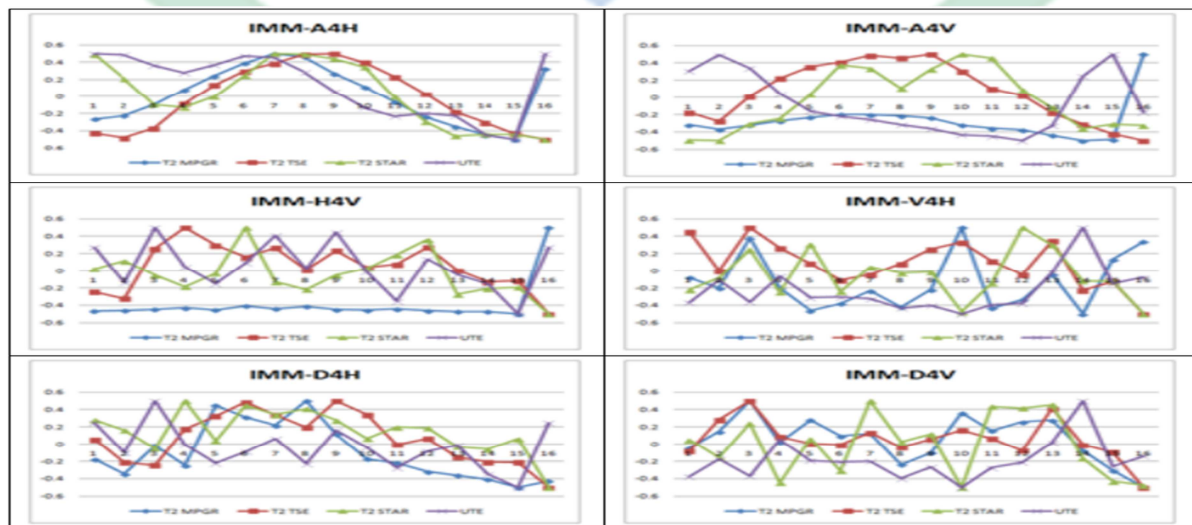
Figure 7. **Analysis of signal in low frequency region after 3 Level DWT immediately after injection of**

C. After 2h of Injection

The T2 pulse sequence and the UTE signal in the acquired image 2 hours after the injection of the contrast agent showed the similar frequency change in the horizontal low frequency signal, vertical low frequency signals showed only different UTE signals. The horizontal high - frequency component showed no change only in T2 MPGR component, vertical high frequency, each diagonal high frequency showed high frequency
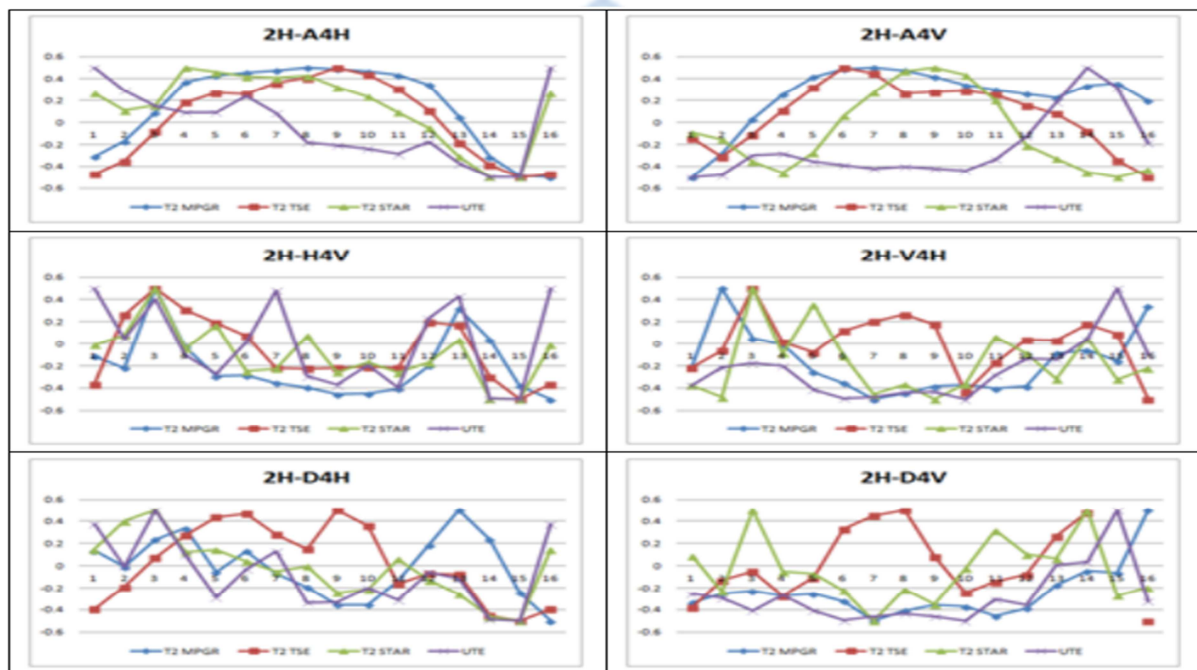
Figure 8. Analysis of signal in low frequency region after 3 Level DWT 2 hours after injection of contrast agent.

D. After 4h of Injection

The T2 pulse sequence and the UTE signal were different from the T2 MPGR signal in the horizontal low frequency signal in the acquired image 4 hours after contrast injection. The remain of the signal appeared in a similar form, vertical low frequency signals differ only in T2 MPGR and UTE signals.

The horizontal high - frequency component showed no change only in T2 MPGR component, vertical high frequency, each diagonal high frequency showed high frequency
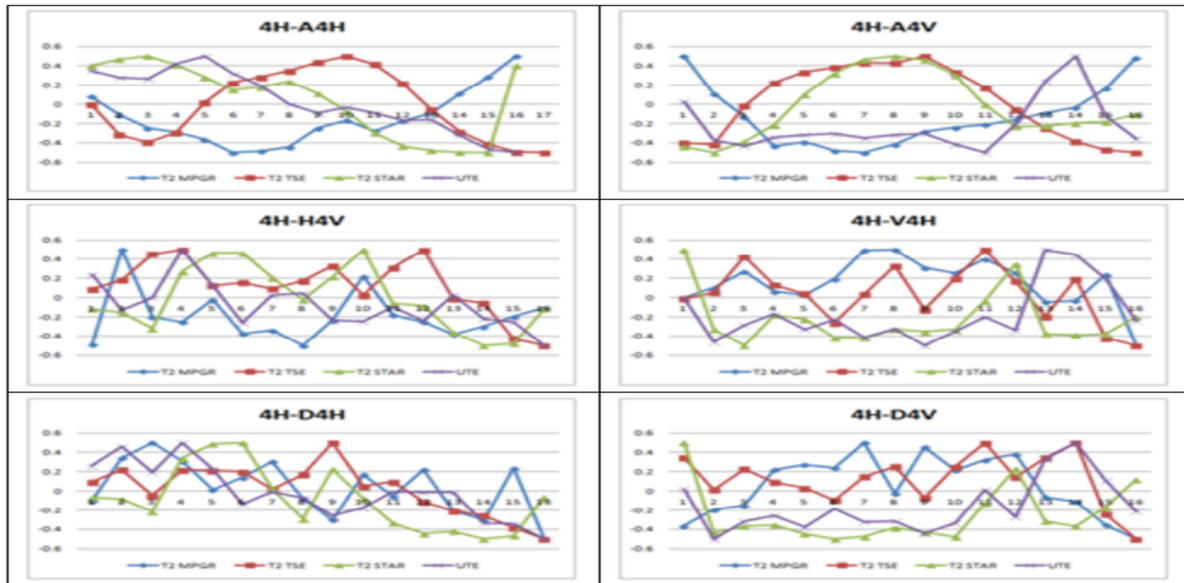
Figure 9. **Analysis of signal in low frequency region after 3 Level DWT 4 hours after injection of contrast agent.**

The UTE pulse sequence is a combination of the characteristics of T2-weighted images that well represent pathologic changes and the characteristics of T1-weighted images that well represent anatomical structures, it is also used as a method to reduce image distortion caused by motion. As a result of analyzing the characteristics of each signal, it is found that in the low frequency region after the 3-level DWT corresponding to the frequency axis of the K-space, the vertical low frequency component in the low frequency region after the 3-level DWT corresponding to the phase axis of the K- Is proportional to TR and TE. The reason why the vertical low-frequency component in the signal before the injection of contrast agent is low in UTE is interpreted as a result of the short signal due to the short TR. Vertical low-frequency components at 2 and 4 hours after injection of contrast medium were lower in T2 MPGR and UTE signals, the reason for this is interpreted as a phenomenon resulting from a small amount of signal emission due to a small number of excited TRs. The horizontal high frequency component and the vertical high frequency component after the 3-level DWT were similar patterns in T2 star and UTE. This is also interpreted as a phenomenon that occurs because the acquisition of T2 star and UTE images is similar to TR and TE. As a result, it was found that the T2 signal and the UTE signal are proportional to TR and TE. Therefore, acquisition of MR molecular image using UTE signal should increase tissue resolution by using nano contrast agent.

Competing interests

The authors declare that there is no conflict of interest regarding the publication of this paper

IV.   Reference

[1] Mahwood U, Emerging Technologies That Will

Change the World : Molecular Imaging. Tech Rev, Vol. 106, 2003.

[2] Chang, Thomas Ming Swi, "Artifical cells", World Scientific Publishing. co. Pte. Lte, 2007.

[3] Byeong-Chole Ahn, Applications of molecular imaging in drug discovery and development process, Curr Pharm Biotechnol, Vol. 12, No. 4, pp.459-468, 2011.

[4] Ho-Taek Song, Jin-Suck Suh, Cancer -Targeted MR Molecular Imaging, J Korean Med Assoc, Vol. 52, pp.121-124, 2009.

[5] Gilad AA, McMahon MT, Walczak P, Winnard PT Jr, Raman V, van Laarhoven HW, Skoglund CM, Bulte JW, van Zijl PC,, Artificial reporter gene providing MRI contrast based on proton exchange, Nat Biotechnol., Vol. 25, pp.217-219, 2007.

[6] A. Yoshitaka, T. Ichkawa, A survey on content-based retrieval for multimedia databases, IEEE Transaction on Knowledge and Data Engineering., Vol. 11, No. 1, 1999.

[7] Jaemoon Yang, Eun-Kyung Lim, Hong Jae Lee, Joseph Park, Sang Cheon Lee, Kwangyeol Lee, Ho-Geun Yoon, Jin-Suck Suh, Yong-Min Huh, Seungjoo Haam,. Fluorescent magnetic nanohybrids as multimodal imaging agents for human epithelial cancer detection., Vol. 20, No. 29, pp.2548-2555, 2008.

[8] Hwunjae Lee, Seung-Hyun Yang, Dan Heo, Hyeyoung Son, Seungjoo Haam, Jin-Suck Suh, Jaemoon Yang, Yong-Min Huh, J of Nanoscience and Nanotechnology., Vol. 16, pp. 196-202, 2016.

[9] Weissleder R and Mahmood U, Molecular imaging, Radiology., Vol. 219, pp.3160-3330, 2001.)(Herschman HR, Molecular imaging : Looking at problems, seeing solutions, Science., Vol. 302, pp.605-608, 2003.

[10] Britz－Cunningham, SHAdelstein SJ, Molecular targeting with radionuclides, State of the science., Vol. 44, pp.1945-1961, 2003.

[11] Strauss LG, Conti PS, The applications of PET in clinical oncology, J Nucl Med., Vol. 32, pp.623-648, 1991.

[12] Rouze NC, Schmand M, Siegal S, Hutchins GD,, Design of a Small Animal PET Imaging System with 1 microliter Volume Resolution, IEEE Trans Nucl Sci., Vol. 51, pp.757-763, 2004.

[13] Jan ML, Chuang KS, Chen GW, Ni YC, Chen S, Chang CH, ET al, A three-dimensional registration method for automated fusion of micro PET-CT_SPECT whole-body images, IEEE Trans Med Imaging., Vol. 24, pp.886-893, 2005.

[14] Joanne E. Holmes, Graeme M. Bydder, MR imaging with ultra short TE (UTE) pulse sequence :

Basic Principles, Radiography., Vol. 11, pp. 163-174, 2005

[15] Maint BA, Elsen PA and Veirgever MA., 3D multimodality medical image registration using morphological tools., Image Vis. Comput Vol. 19, p.53-62, 2001.

[16] H. Kauppinen, T. Seppanen, M. Pietikainen, "An experimental comparison of Autoregressive and Fouier-Based Descriptors in 2D shape Classification", IEEE Transaction on PAMI, Vol.17, No.2, pp.201-207, February. 1995.

[17] Sangbock Lee, Junhaeng Lee, Taesil Kim, "Disease Recognition on Medical Images Using Neural Network", Journal of Korean Society of Radiology, Vol. 3, No. 1, PP. 27~36, 2009.

[18] I. Daubechies, "Orthonomal bases of compactly supported wavelets", Co- mmun. Pure Appl. Math., Vol. 41, No. 7, PP. 909-996, 1988.

[19] Stephane G. Mallat, "A theory for multiresolutional signal decomposition; the wavelet representation", IEEE trans. Pattern Anal. Machine Intell., Vol. 11, No. 7, PP. 674-693, July, 1989.

Ingrid Daubechies, "Ten Lectures on Wavelets", SIAM, 1994.

Blank Page

MR Molecular Imaging Based on Magnetic Nanoparticles

SangBock Lee[1], Geyhwan Jin[2], Sergey NETESOV[3], Giljae Lee[4]*

Abstract The development of synchronized delivery and imaging system for small interfering RNA (siRNA) is required for the clinical application of RNA interference (RNAi) in cancer treatment. In this paper, we propose a pH-responsive, magnetic nanoparticle-based siRNA delivery system that can facilitate the safe and efficient delivery and visualization of therapeutic siRNA by high resolution magnetic resonance (MR) imaging.

The synthesized nanovectors were then complexed with siRNA targeting the CD44 gene via electrostatic interaction to verify the specific gene-silencing effect. The imidazolized magnetic nanovector (ImMNV) architectures developed here facilitated improved cellular internalization and exhibited a high level in vitro down regulation compared to non-imidazolized magnetic nanovectors in metastatic breast cancer cells.

[1*]SangBock Lee(✉)   ***corresponding author***

Dept. of Radiology, Nambu University, (62271) 23 Chumdan Jungang-ro, Gwangsan-gu, Gwangju, , Korea

[2]Geyhwan Jin

Dept. of Radiology, Nambu University
e-mail : ghjin@nambu.ac.kr

Sergey NETESOV[3]
Dept. of Biotechnology , N S U
e-mail : Netesov-s@nsu.ru

[4]Giljae Lee

Department of Radiology, Nambu University, Graduate School
e-mail : korotkoff@korea.kr

I.   Introduction

RNA interference (RNAi), a post-transcriptional mechanism of specific gene regulation, is a natural cellular process whereby small RNA duplexes (or small interfering RNAs; siRNAs) targeting specific genes inhibit protein production by exerting translational repression or triggering the direct degradation of target messenger RNA (mRNA)[1][2]. With its ability to specifically and potently silence any target genes at the RNA level, RNAi affords great opportunities to lay the foundation for a breakthrough product that would be able to rapidly generate novel therapeutics[1][2]. Despite its abundant promise, however, a number of issues and challenges remain for RNAi-based therapeutics, the most import concern being the safe and effective delivery of siRNA to the cells and tissues in the body. In other words, the success of RNAi-based

therapy largely depends on the rational engineering of delivery vectors that contain functionalities such as targeting moieties, stimuli-response components, and stability enhancers[3][4][5]. Synthetic materials including cationic polymers (i.e., polylysine, polyethyleneimine, polyamidoamine, poly-β-amino esters, chitosan, etc.) have been used to condense siRNA molecules, and as a backbone for further modification with functional groups (i.e., targeting ligands, stimuli-responsive linkages, etc.) or neutral charged polymers to trigger siRNA release and to substantially reduce cytotoxic effects. In either case, the delivery carrier is mainly routed to endosomes/lysosomes and experiences a decrease in pH from physiological to lysosomal pHs. The internalized siRNA molecules, therefore, should rapidly escape into the cytosol, which is regarded as the major limitation of the transfection efficiency of synthetic material-based vectors. Several strategies have been built to overcome this unavoidable step and include the incorporation of fusogenic characters (i.e., GALA peptide, imidazole, etc.) In particular, the introduction of pH-dependent imidazole residues (pKa ~6.0) into various polycations could promote the destabilization of endosomal membranes, because an imidazole ring can be easily protonated in the endosomal environment. Although imidazole-containing polymers showed reduced binding strength with siRNA due to weak positive charge density per molecule compared to free amine-containing ones, they still offer numerous interesting perspectives for the design of a promising platform for siRNA delivery. Schematic illustration of the synthesis of pH-responsive imidazolized magnetic nanovectors (ImMNV) with cationic polymer (PLI) and magnetic nanoparticles (MNPs) through the emulsion process, and the formation of ImMNV/siRNA complexes via electrostatic interaction. Schematic illustration of a rapid change in the surface charge of ImMNV in response to a reduction in pH as a result of pH-activated protonation of imidazole rings.
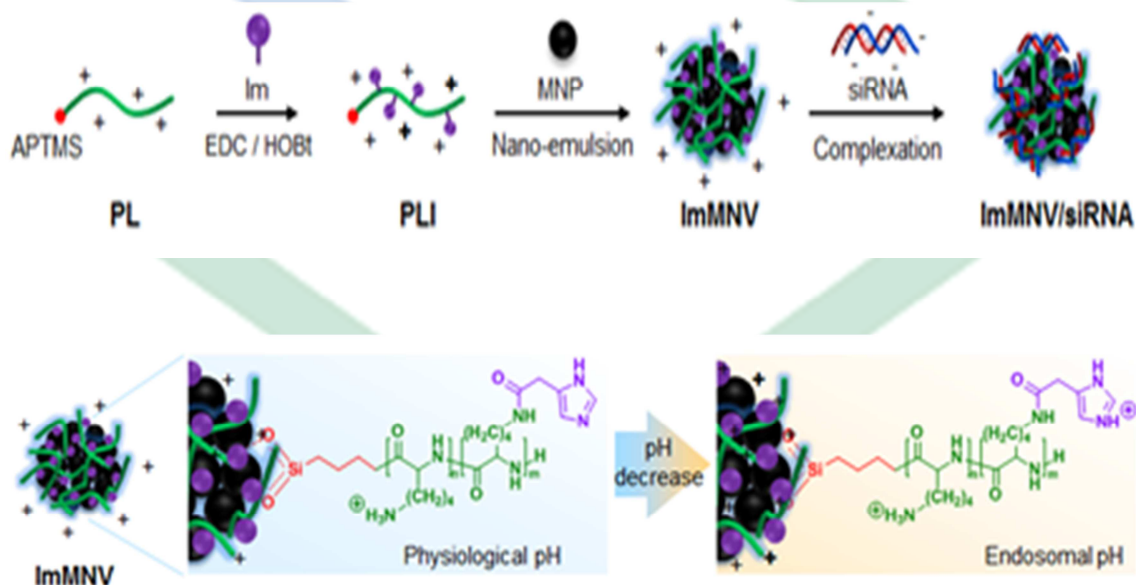
II. Materials and methods

N6-carbobenzyloxy-L-lysine (LysZ), 4-imidazoleacetic acid, (3-aminopropyl)trimethoxysilane (APTMS), 1-ethyl-3-N,N-dimethylaminopropyl carbodiimide (EDC) hydrochloride, trifluoroacetic acid (TFA),

hydrobromic acid solution (33 wt % in acetic acid) (HBr/AcOH), anhydrous tetrahydrofuran (THF), N,N-dimethylformamide (DMF), dimethylsulfoxide (DMSO), 1N sodium hydroxide (NaOH) solution, iron (III) acetylacetonate, manganese (II) acetylacetonate, 1,2-hexadecanediol, lauric acid, lauryl amine, benzyl ether, deuterium oxide (D2O), and dimethylsulfoxide-d6(DMSO-d6)werepurchasedfromSigma-Aldrich(St.Louis,MO, USA). Triphosgene was obtained from Tokyo Chemical Industry Co. (Tokyo, Japan), and 1-hydroxybenzotriazole hydrate (HOBt) was obtained from Daejung Chemicals & Metals Co. (Shiheng, Korea). n-Hexane and diethyl ether were purchased from Ducksan Scientific Co. (Seoul, Korea) and Samchun Pure Chemical Co. (Seoul, Korea), respectively. The CD44-specific siRNA (siCD44) (sense: 5´-CAGAUAGGCAAGUUUAUGA-3´, antisense: 5´-UCAUAAACUUGCCUAUCUG-3´) and negative control siRNA (siNC) (sense: 5´-CCUACGCCACCAAUUUCGU-3´, antisense: 5´-ACGAAAUUGGUGGCGUAGG-3´) were purchased from Bioneer Co. (Daejeon, Korea).

1. Fabrication of PLI-coated magnetic nanovectors (ImMNVs)

Imidazolized magnetic nanovectors (ImMNVs) as potential siRNA carriers and MR imaging agents were prepared by the nano-emulsion method.

Firstly, monodisperse manganese ferrite (MnFe2O4) nanoparticles (MFs) were synthesized by the thermal decomposition of metal-organic precursors in the presence of nonpolar organic solvents.[26] In detail, iron (III) acetylacetonate (2 mmol), manganese (II) acetylacetonate (1 mmol), 1,2-hexadecanediol (10 mmol), lauric acid (6 mmol), and laurylamine (6 mmol) were dissolved in 20 mL of benzyl ether. The solution was preheated to 200°C for 2 hr under an ambient nitrogen atmosphere and refluxed at 300°C for 1 hr. After cooling the reactants to room temperature, the products were purified using an excess of pure ethanol. Approximately 11-nm MFs were synthesized using the seed-mediated growth method. Twenty milligrams of the as-synthesized MFs were dissolved in 4 mL of n-hexane and subsequently added into 20 mL of DW containing 50, 100, or 200 mg of PLI (ImMNVs2.5, ImMNVs5, and ImMNVs10). After mutual saturation of the organic and aqueous phases, the mixture was ultrasonicated at 190 W for 15 min with vigorous stirring at 1,200 rpm, and stirred for 4 hr to evaporate the residual hexane. It was then collected by sequential centrifugation under three different conditions (at 15,000 rpm for 30 min, at 8,000 rpm for 15 min, and at 5,000 rpm for 15 min) to reduce the size distribution of the polydispersed ImMNVs.

2. Characterizations of ImMNVs

The average hydrodynamic diameters and zeta

potentials of the obtained ImMNVs were measured using dynamic laser scattering (ELS-Z, Otsuka Electronics, Osaka, Japan) at room temperature. Their size distributions and morphologies were observed by transmission electron microscopy (TEM, JEM-2100 LAB6, JEOL Ltd., Tokyo, Japan) at an accelerating voltage of 200 kV. The concentration of Mn plus Fe ions in the ImMNVs was measured by using inductively coupled plasma-atomic emission spectrometry (ICP-AES) analysis (IRIS Intrepid II XSP, Thermo Fisher Scientific, Boston, MA, USA). The magnetic hysteresis loop and the saturated magnetization value were obtained using a vibrating sample magnetometer (VSM, MODEL-9407, Lake Shore Cryotronics, Inc., Westerville, OH, USA) at 25°C. The amount of MFs or polymeric coatings encapsulated in ImMNVs and MNVs was measured by thermal gravimetric analysis (TGA, SDT-Q600, TA instrument, New Castle, DE, USA). The T2 relaxivity (r2) data of the ImMNV solution were obtained through magnetic resonance (MR) imaging analysis.

3. Preparation of siRNA-loaded ImMNVs

ImMNVs/siRNA complexes were formulated by briefly vortexing siRNA stock solution (10 μM) in diethylpyrocarbonate (DEPC)-treated water with the desired amount of ImMNVs, corresponding to different weight ratios of polycations to siRNA (5 to 25), for a final siRNA concentration of 0.5 μM. After mixing, the complexes were incubated for 15 min at room temperature. The siRNA condensation ability of ImMNVs was confirmed by the gel retardation assay. To compare siRNA-loading ability, siRNA was also complexed with varying amounts of MNVs. The prepared complexes were mixed with 6× HiQTM goRed (Genepole, Seoul, Korea), then loaded into a 2% agarose gel (w/v), and electrophoresed in Tris-borate-EDTA (TBE) buffer at 100 V for 20 min. The retardation of complexes was visualized by a UV lamp using a Gel Doc System.

4. Cell viability test

The cytotoxicity of ImMNVs and MNVs in breast cancer MDA-MB-231 cells was evaluated by a colorimetric assay, based on the cellular reduction of 3-(4,5-dimethylthiazoly-2)-2,5-diphenyltetrazolium bromide (MTT) (Cell Proliferation Kit I, Roche, Germany) in metabolically active cells. MDA-MB-231 cells (1 × 10^4 cells/well) were seeded into 96-microwell plates, incubated in RPMI 1640 medium containing 5% fetal bovine serum (FBS) and 1% antibiotics at 37°C overnight in a humidified atmosphere with 5% CO_2, and then treated with ImMNVs and MNVs containing medium with 5% FBS at various concentrations for additional 24 hr. After incubation, the yellow MTT solution was added and the formazan crystals formed were solubilized with 10% sodium dodecyl sulfate in 0.01 M HCl. Then the relative percentage of cell viability was calculated from the formazan intensity ratio of treated to non-treated control cells and shown as an average ± standard deviation (n = 4).

5. MR imaging procedures

We performed solution and in vitro MR imaging experiments with a 1.5 T clinical MRI instrument with a micro-47 surface coil (Intera, Philips Medical Systems, Best, The Netherlands). The R2 (T2 relaxation rate, $1/T2$, s^{-1}) of the ImMNV solution and ImMNV- or MNV-treated cells (1×10^7) were measured by using the Carr-Purcell-Meiboom-Gill (CPMG) sequence at room temperature with the following parameters: TR = 10 sec, 32 echoes with 12 msec even echo space, number of acquisitions = 1, point resolution of 156×156 μm, and section thickness of 0.6 mm. For the acquisition of T2-weighted MR images of ImMNVs solution and ImMNVs- or MNVs-treated cells, the following parameters were adopted: resolution of 234×234 μm, section thickness of 2.0 mm, TE = 15 msec, TR = 400 msec, and number of acquisitions = 1. The r2 ($mM^{-1}s^{-1}$) is equal to the ratio of the R2 to the ImMNV or MNV concentration.

6. Cellular uptake of ImMNVs

To prepare cellular TEM samples, MDA-MB-231 cells (1×10^6) were harvested after TrypLETM (Gibco®) treatment, washed in triplicate with blocking buffer (0.03% bovine serum albumin and 0.01% NaN^3 in phosphate-buffered solution, pH 7.4 and 10 mM) to prevent non-specific binding, and gently pelleted. Subsequently, the cells were suspended in ImMNV solution (0.46 μg/mL) and

incubated for 30 min on ice and 30 min at 37℃. After incubation, the cells were washed three times with blocking buffer and fixed according to the standard fixation and embedding protocol for resin-section TEM. The sample resin blocks were trimmed and sectioned using a LEICA Ultracut UCT Ultra-microtome (Leica Microsystems Ltd., Austria). Cellular uptake of ImMNVs was also examined by the Prussian blue staining method. To stain magnetic components in MDA-MB-231 cells treated with ImMNVs (0.46 μg/mL), the cells were incubated with 2% potassium ferrocyanide in 10% HCl and then counterstained with Nuclear Fast Red (Sigma-Aldrich). Cellular internalization of the ImMNVs was observed by TEM (JEM-1011, JEOL Ltd., Tokyo, Japan) at an accelerating voltage of 80 kV and an epi-fluorescence microscope (BX51 upright microscope, Olympus, Japan).

7. In vitro transfection and quantitative reverse transcriptase-polymerase chain reaction (qRT-PCR) analysis

To measure CD44 mRNA expression levels in breast cancer cells, real time qRT-PCR analysis with internal standards was performed. Firstly, MDA-MB-231 cells (2×10^5 cells/well) were seeded in six-well plates containing 2 mL culture medium supplemented with 10% FBS and incubated at 37℃ overnight to reach 70% confluence at the time of transfection. The culture medium was then replaced with serum-free medium and 100 μL of ImMNVs or MNVs

containing siCD44 or siNC (100 pmol) at a polycation/siRNA weight ratio of 1:2 was added to each well. As a control, MDA-MB-231 cells were also transfected with free siCD44 or siNC. After a 6-hr incubation, the medium was replaced with 2 mL fresh culture medium and further incubated at 37℃ for 48 hr. The cells were harvested 48 hr after transfection, and total RNA was isolated from the cells with the RNeasy® Plus Mini Kit (QIAGEN, Hilden, Germany), according to the manufacturer's instructions. Complementary DNA (cDNA) was synthesized from 2 μg of total RNA using the High Capacity RNA-to-cDNA kit (Applied Biosystems®). The resulting cDNA was amplified by PCR, conducted with the QuantiMix SYBR Kit (PhileKorea Technology, Daejeon, Korea) on a real-time PCR system (LightCycler® 480 System, Roche). Primer sequences were as follows: CD44, forward 5´-CCTCTT GGCCTTGGCTTTG-3´ and reverse 5´-TCCATTGCCACTGTTGATCA-3´; GAPDH, forward 5´-GCTCTCTGCTCCTCCTGTTC-3´ and reverse 5´-TGACTC CGACCTTCACCTTC-3´. The PCR conditions were as follow: initial denaturation at 95℃ for 10 min; 45 cycles of amplification at 95℃ for 10 sec, at 60℃ for 10 sec, and at 72℃ for 10 sec. Each sample was performed in triplicate. The relative CD44 mRNA expression value was normalized to the endogenous reference gene (GAPDH) in the corresponding samples and relative to non-treated cells, and calculated by the ΔΔCt method.

8. Western blot analysis

To assess the down-regulation of the CD44 gene in MDA-MB-231 cells, the cells were harvested and lysed in cold RIPA buffer (Pierce®, Thermo Scientific) containing a protease inhibitor cocktail tablet (cOmplete Mini, Roche). The lysates were incubated at 4℃ for 30 min and centrifuged at 13,000 rpm for 15 min. The supernatants were analysed for protein concentrations using the bicinchoninic acid (BCA) Protein Assay (Pierce®). Equal amounts (20 μg) of protein were subjected to electrophoresis on sodium dodecyl sulfate (SDS)-polyacrylamide gels and then transferred to a nitrocellulose blotting membrane (Amersham ™ Hybond ECL, GE Healthcare). The blotted membranes were immunostained with antibodies specific for CD44 (156-3C11, Cell Signaling Technology, Inc., USA) and GAPDH antigens (6C5, Santa Cruz Biotechnology, Inc., USA). The signals were developed by a standard enhanced chemiluminescence (ECL) method (Pierce® ECL Plus Western Blotting Substrate) according to the manufacture's protocol.

III. Results and discussion

1. Preparation of imidazolized magnetic nanovectors (ImMNVs)
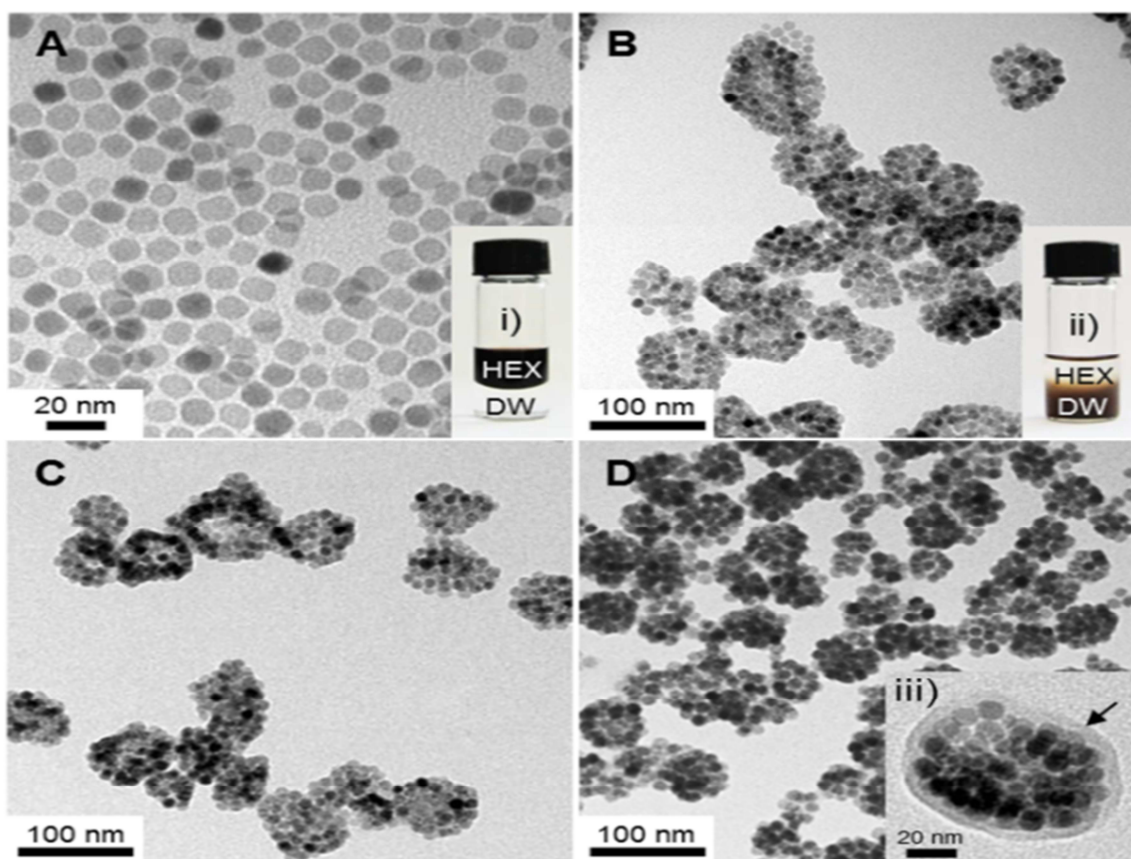
Fig. 1. TEM images of (A) lauric acid coated MFs, (B) ImMNVs2.5, (C) ImMNVs5.0, and (D) ImMNVs10.

Fig. 1. show photographs of (i) MF dispersed in hexane (HEX) and (ii) ImMNV2.5 dispersed in distilled water (DW); in (iii) the image of ImMNV10 at higher magnification indicating the surface layer is clearly visible.

Based on the obtained TEM images, MFs have a highly uniform size of 11.3 ± 1.0 nm (100 particles were measured) and the formulated ImMNVs show spherical and densely packed clusters of MFs with an average size of 61.7 ± 9.0 for ImMNV2.5, 61.3 ± 8.6 for ImMNVs5, and 49.2 ± 2.9 nm for ImMNVs10. Closer examination of a single nanoparticle in the TEM image of ImMNVs10 revealed that multiple MFs were densely clustered and covered by a thin polymeric layer (~6 nm, indicated by an arrow). Non-imidazolized MNVs (MNVs) showed heterogeneous nanoclusters with irregular forms in their TEM image and a 1.3-fold increase in hydrodynamic diameter compared with ImMNVs. suggesting that PL segments alone seem to be not sufficient to stabilize the entire surface area of MFs due to the less hydrophobicity than PLI under neutral pH conditions.
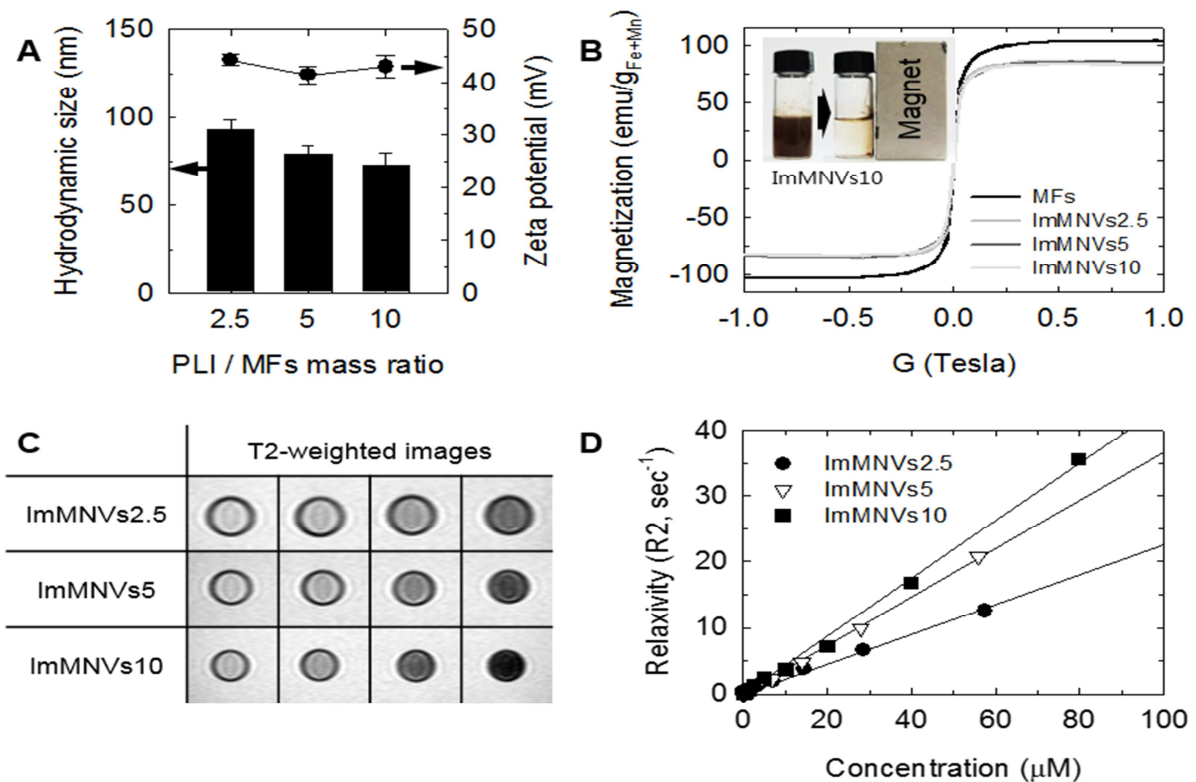
Fig. 2 Characteristics of ImMNVs as MR contrast agents.

(A) Size and zeta potential of ImMNVs prepared at various PLI/MFs mass ratios (2.5, 5, and 10). (B) Magnetic hysteresis curves of MFs and ImMNVs measured by a vibration sample magnetometer. The inset shows the magnetic sensitivity of ImMNVs10 using the Nd-Fe-B magnet. (C) T2-weighted MR images of ImMNVs in aqueous solution and (D) plots of relaxivity (R2) against ImMNV concentration.

The average hydrodynamic sizes and zeta potentials of theses ImMNVs dispersed in DI (pH 5.5) were measured using laser scattering (Fig. 2a). Overall, as the mass ratio of PLI to MFs increased from 2.5 to 10, the particle sizes slightly decreased from 93.0 ± 6.0 nm to 72.9 ± 7.1 nm, which was quite consistent with the trend in their sizes as obtained from TEM images. The hydrodynamic size of ImMNVs measured by laser scattering was larger than the value obtained from TEM because of the swelling of hydrophilic PLI polymer under the aqueous environment. It should be noted that the protonation state of the side chain of PLI changes from non-protonated imidazole to protonated imidazolinium or imidazolium in response to endosomal acidification. To assess the potential use of ImMNVs as MR imaging contrast agents, we investigated the MR images and the T2 relaxivity (R2) of variously prepared ImMNVs at different concentrations using a 1.5 T MRI instrument (Fig. 2c and 2d). As the concentration of MFs (Fe + Mn ions) in ImMNVs increased, the T2-weighted MR images were linearly darkened and the

corresponding r2 values of ImMNVs2.5, ImMNVs5, and ImMNVs10 were 224.5, 367.2, and 437.1 mM^{-1}s^{-1}, respectively. From these data, we demonstrated that ImMNVs10 revealed an efficient gene-loading capacity and a remarkably high MR contrast effect, and was thereby chosen for further in vitro experiments.

2. Cell viability and intracellular uptake

We next examined the in vitro differential toxicity of the prepared nanovectors using the MTT assay on the breast cancer cell line MDA-MB-231. The cells were treated with MNVs and ImMNVs at concentrations ranging from 10^{-7} to 10^{-1} mg Fe+Mn/mL and incubated for 24 hr. The cell viability in Fig. 3a showed that both MNVs and ImMNVs exhibited no significant proliferation inhibition (over 80% cell viability) up to 0.1 mg/mL with 24 hr incubation. We further evaluated the MR contrast effect of MNVs and

ImMNVs in MDA-MB-231 cells using MR imaging at 1.5 T. In the T2-weighted MR images, a significant enhancement in T2 signals was obtained in ImMNVs-treated cells compared to non-treated control cells (Fig. 3b). ImMNVs were more efficiently taken up than MNVs, probably due to the higher zeta potential and r2 values of ImMNVs, as described by laser scattering and solution MR analysis. In the TEM images, the considerable amount of black clusters in MDA-MB-231 cells treated with ImMNVs implies the internalization of ImMNVs into the cytoplasm without damaging cellular structures (Fig. 4a and 4b). The images from Prussian blue staining showed similar results. Numerous blue spots, produced by the rapid exchange of electrons between Prussian blue and the ferric ions of the MFs, appeared in the intracellular region (Fig. 4c and 4d). Collectively, these results indicated that ImMNVs are suitable for use as an MR nanoprobe for versatile imaging and ultrasensitive detection at the cellular level.
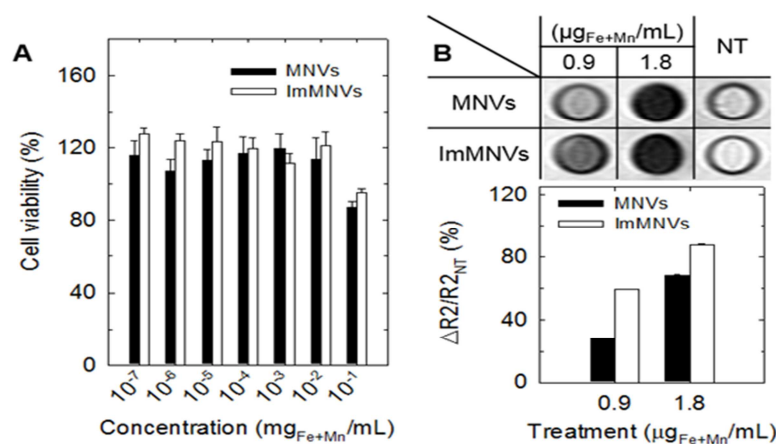
Fig. 3. (A) Cell viabilities of MDA-MB-231 cells treated with different concentrations of MNVs and ImMNVs. (B) T2-weighted MR images and the graph of ΔR2/R2NT of MDA-MB-231 cells incubated with and without MNVs and ImMNVs, respectively
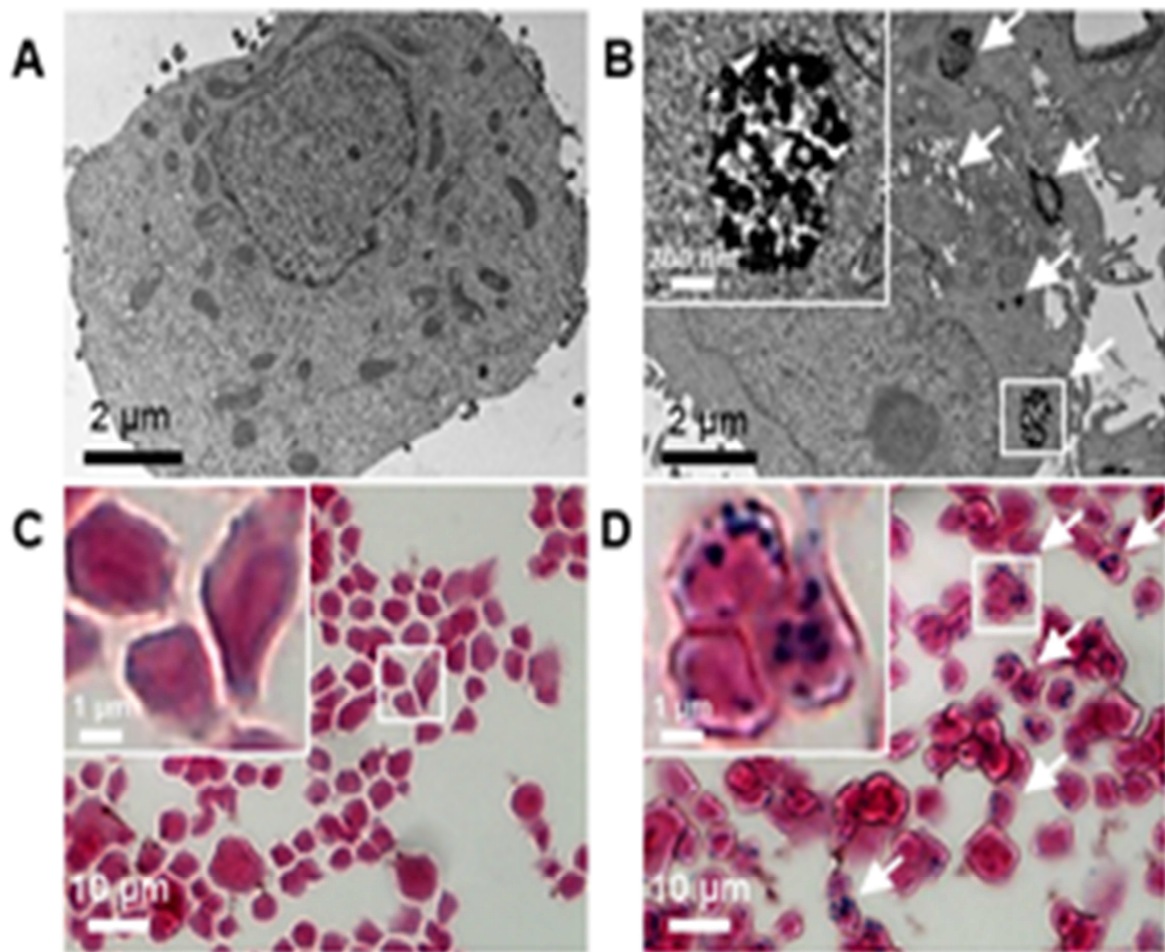
Fig. 4. Cellular TEM images and Prussian blue-stained images of MDA-MB-231 cells treated (A, C) without and (B, D) with ImMNVs. The insets show the magnified images of white boxes and the white arrows indicate the presence of ImMNVs in the cells.

3. In vitro gene silencing

To verify the potential utility of the ImMNV formulation for siRNA-based cancer therapy, the gene silencing ability of ImMNVs was investigated in metastatic breast cancer cells. MDA-MB-231 cells express high levels of the CD44 receptor, a significant prognostic biomarker of metastatic cancer, and its upregulation is highly relevant to tumor cell metastasis and invasion. Thus, these cells are appropriate for use in this study to determine

therapeutic effect by knockdown of a specific gene set. In addition, this siRNA delivery system based on inorganic nanoparticles and polycations is expected to facilitate improved delivery efficiency through the process of endocytosis and an enhanced gene silencing effect by rapid endosomal escape from endosomes. Therefore, the relative expression levels of CD44 mRNA in MDA-MB-231 cells after treatment with ImMNVs containing siRNA targeting the CD44 gene (siCD44) or negative control siRNA (siNC) respectively were examined by real-time qRT-

PCR analysis. For comparison, MNVs that lack imidazole groups were complexed with siCD44 or

siNC and used in the transfection experiments.
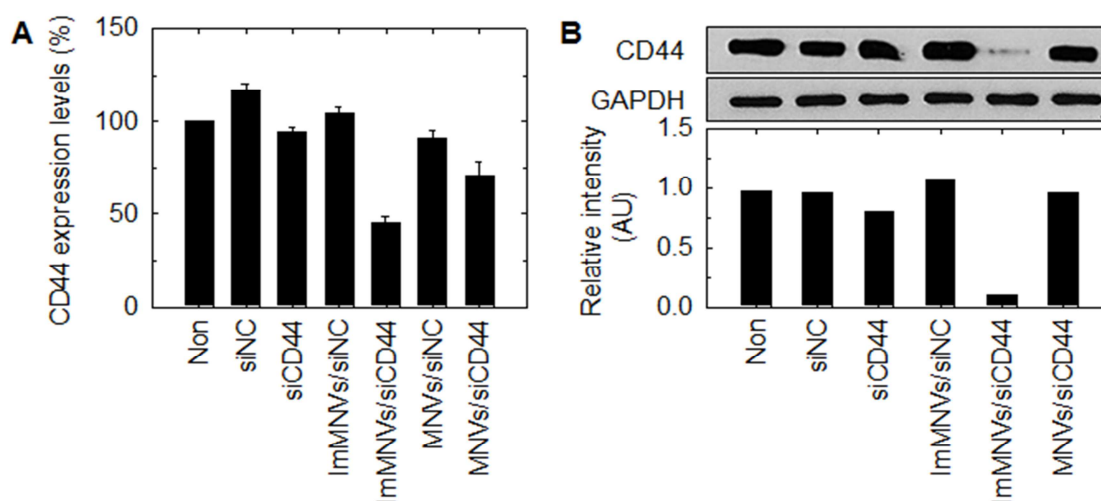
Fig. 5. Specific gene-silencing effect of MNVs/siCD44 complexes. (A) Relative expression of CD44 mRNA in MDA-MB-231 cells incubated with ImMNVs and MNVs containing siNC or siCD44, respectively. The relative mRNA expression levels (%) by qRT-PCR analysis were normalized to the mRNA level of endogenous GAPDH in the same sample. (B) Western blot analysis of CD44 from whole cell lysates of MDA-MB-231 cells treated with ImMNVs and MNVs containing siNC or siCD44 using GAPDH as a loading control. Non-treated cells were used as a negative control.

As shown in Fig. 5a, ImMNVs/siCD44 complexes clearly reduced CD44 expression by more than 54% in these cells, compared with untreated cells as well as siNC- or siCD44- treated cells. This effect is about 2-fold higher than that seen with MNVs/siCD44 complexes. In contrast, the corresponding amount (100 pmol) of siNC combined with ImMNVs did not exhibit any silencing effect, indicating target-specific gene inhibition. We further confirmed the protein expression levels of CD44 using Western blot analysis upon treatment of the cells with different conditions (Fig. 5b). As expected, CD44 protein expression had similar tendencies as observed in

the qRT-PCR results. Obviously, the lowest expression of CD44 was observed in cells treated with ImMNVs, relative to other treatment groups, confirming that ImMNV-mediated intracellular delivery of siCD44 could potentially downregulate the expression of a specific gene in CD44-overexpressing cells at both the post-transcriptional and protein levels.

IV. Conclusions

In summary, we present the development and feasibility of an imidazolized magnetic nanovector (ImMNV) for the efficient delivery of therapeutic

siRNA and simultaneous detection of cancer by MRI. A rationally engineered cationic polymer, PLI, as a robust stabilizer was utilized to successfully form water-dispersible magnetic nanoclusters with cationic polymeric shells, producing a stable polyelectrolyte complex through electrostatic interaction. These ImMNVs optimized by controlling the amount of PLI in the emulsion process, showed high MR sensitivity due to their clustering effect and exhibited significant enhancement in T2 signals compared to non-imidazolized MNVs. We verified the in vitro specific gene knockdown effects of ImMNVs in MDA-MB-231 cells using both qPCR and Western blot analyses. Consequently, our proposed pH-responsive gene delivery and imaging system would be beneficial to expand research on magnetic nanoparticle-based theranostics for cancer treatment.

[Reference]

[1] A.L Jackson, S.R Bartz, J. Schelter, S.V. Kobayashi, J. Burchard, M. Mao, B. Li, G. Cavet and P.S. Linsley, "Expression profiling reveals off-target gene regulation by RNAi", *Nat. Biotechnol.*, 2003, *21*, 635-637.

[2] R. S. Kamath, A. G. Fraser, Y. Dong, G. Poulin, R. Durbin, M. Gotta, A. Kanapink, N. L. Bot, S. Moreno, M. Sohrmann, D. P. Welchman, P. Zipperlen and J. Ahringer, "Systematic functional analysis of the Caenorhabditis elegans genome using RNAi", *Nature*, 2003, *42*, 231-236

[3] D. W. Pack, A. S. Hoffman, S. Pun and P. S. Stayton, "Design and development of polymers for gene delivery", *Nat. Rev. Drug Discov.,* 2005, *4*, 581-593.

[4] S. Mura, J. Nicolas and P. Couvreur, "Stimuli-responsive nanocarriers for drug delivery", *Nat. Mater.*, 2013, *12*, 991-1003.

[5] D. Luo and W.M. Saltzman, "Enhancement of transfection by physical concentration of DNA at the cell surface", *Nat. Biotechnol.*, 2000, *18*, 33-37.

[6] Hoffman JM, Menkens AE. "Molecular imaging in cancer: future directions and goals of the National Cancer Institute". Academic radiology 2000;7(10):905-907.

[7] Nishino M, Jackman DM, Hatabu H, Janne PA, Johnson BE, Van den Abbeele AD. "Imaging of lung cancer in the era of molecular medicine". Academic radiology 2011;18(4):424-436.

[8] Kiessling F. "Science to practice: the dawn of molecular US imaging for clinical cancer imaging", Radiology 2010;256(2):331-333.

[9] Pinker K, Stadlbauer A, Bogner W, Gruber S, Helbich TH. "Molecular imaging of cancer: MR spectroscopy and beyond", European journal of radiology 2012;81(3):566-577.

[10] Guyrack Choi, Sangbock Lee, "Application and Prospects of Molecular Imaging", J. Korean. Soc. Radiol., Vol. 8, No. 3, April 2014, pp. 123~136.

OPEN ACCESS

T2-weighted MRI of breast cancer using hyaluronic acid coated magnetic nanoparticles as a tool of contrast agent

Sangbock Le [a] ,e[b+], Hwayeon Yeo[b], Byungju Ahn, [b], V. R. Singh [c], Nguyen Van Do [d]

ABSTRACT Novel diagnostic technique has been developed in many research area using targetable contrast agents with magnetic resonance imaging (MRI) for cancer diagnosis. It is efficient for cancer diagnosis to use MRI with biocompatible targeting moiety and magnetic nanoparticles (MNPs). Thus, we synthesized MNPs using thermal decomposition method which enable sensitive T2- or T2 Turbo spin echo (TSE) weighted magnetic resonance imaging.

[a, b+]S. B. Lee ✉
Correspondence to: Sangbock Lee
Dept. of Radiology, Nambu University

[b]Hwayeon Yeo
Dept. of Radiology, Nambu University
e-mail : yhy@gmail.com

[b]Byungju Ahn
Dept. of Radiology, Nambu University
e-mail : anju6010@gmail.com

[c]V. R. Singh
Director, PDM University, India
e-mail : vr-singh@ieee.org

[d]Nguyen Van Do
Dept. of Nuclear Engineering, Hanoi University of Science and Technology
e-mail : vr-nguyen.van.do@hust.edu.vn

And it was coated with Hyaluronic acid (HA). Also we carried out that breast cancer cell line (MDA-MB-231) which has cancer stem cell property was injected in heterotopic mouse model. And then magnetic resonance sequence (T2) for imaging effects and targeting ability were analyzed into MNPs conjugated HA. We noted that MDA-MB-231 cell which high-expressed CD44 ligand was showed contrast enhance efficiency through magnetic nanoparticles because of combining a lot of HA As a result of these studies, we conclude that HA coated magnetic nanoparticles can be effectively used as a novel probe for visualizing of Breast cancer stem cell.**Key words**: contrast agent, gastric cancer, CD44, magnetic nanoparticles, magnetic resonance imaging

Keywords : T2-weighted MRI, Hyaluronic acid coating, Magnetic Nano Particles, Contrast Agents

1. Introduction

Molecular imaging provides as a tool to diagnose cancer at the cellular and molecular levels. It not only allows early and accurate tumor localization in diagnostic cancer imaging, but also has a potential to visualize the biological processes of tumor growth, metastasis and response to treatment.(1-10) Molecular MR imaging (Magnetic resonance imaging) has emerged as a key factor for the diagnosis of cancer.(11-18) Since it has advantages over noninvasive, good anatomical image due to high resolution,

high contrast and 3-dimensional information in real time more than nuclear medicine (PET, SPECT), optical imaging compared to other imaging modality.(19-23) And also, molecular MR imaging is able to detect simultaneously metabolism of cells and tissues and its physiological information and structural information, noninvasive and biological processes occurring in the deep tissues to provide the quantitative information.(24,25) Molecular MR imaging can observe a variety of imaging lesions as multi-modality in the diagnosis of breast cancer.

Many MR contrast agents have been used for good quality imaging (32-37). However passive contrast agents are not enough to reach their target goals specifically. Thus, we are aiming to develop intelligent targetable contrast agent using Hyaluronic acid (HA)(38-44). In particular, HA has become known to interact on CD44 receptor. Then breast cancer is known to being overexpressed CD44 receptor which as marker of cancer stem cell.(44) It is so crucial for MR probe to early breast cancer diagnostic point of view. Because CD44, important as cancer stem cell marker, is interacted with Hyaluronic acid. Hyaluronic acid which is a linear hydrogel with negative charge containing two alternating units of D-glucuronic acid (GLcUA) and N-acetyl-D-glucosamine (GLcNAc) with molecular weight of 105–107. HA has frequently been used for medical purposes such as a viscoelastic biomaterial in surgery.

Especially, it is well known that various human tumor cells (breast, ovarian, colon, lung, stomach, etc.) over-express HA-binding receptors, CD44 (44) In this study, molecular MR imaging were investigated to find biological processes which occur in gastric cancer. T2 weight sequence was simultaneously used to confirm for better diagnostic possibility and targeting effect was demonstrated through Hyaluronic acid conjugated magnetic nanoparticles in heterotopic xenograft breast cancer model. And various experiments were conduct to evaluate specific binding affinity and diagnostic effectiveness through in vivo and in vitro.

2. RESULT AND DISCUSSION

2.1 Preparation of MNPs and HA-MNPs

Monodispersed magnetic nanoparticles were synthesized using thermal decomposition and solubilized in nonpolar organic solvent, as previously reported. And HA conjugated MNP was synthesized using EDC and sulfo-NHS method. As shown in (Fig. 1), the characteristic band of HA-MNPs conjugates were verified by FT-IR spectra, which exhibits O-H stretching at $3200-3400 cm^{-1}$, C=O stretching at $1100-1300 cm^{-1}$, CO-NH(amide) bonds at $1630-1680 cm^{-1}$ and CH_2 bending in HA at $1430-1470 cm^{-1}$.
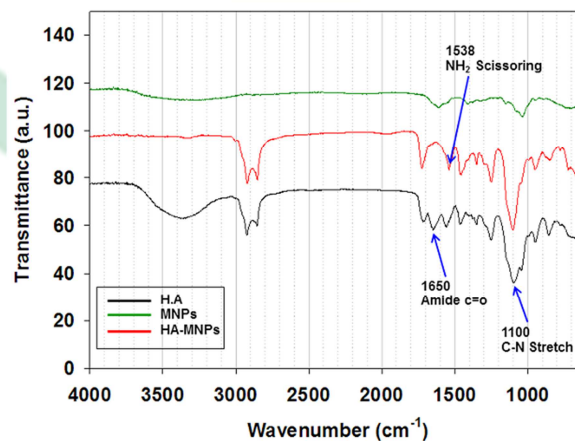
Fig.1. Fourier transform infrared spectra of HA (green line), MNP (red line) and HA-MNP(black line), i:CO-NH(amide) bonds

As MR agents, uniform MNPs (12nm) were synthesized at a high temperature via a thermal decomposition process. The size distribution and morphology of MNPs were

confirmed by transmission electron microscopy (Fig. 2.) which showed no significant differences in size or morphology between HA-MNPs and MNP. The size of the

water-soluble MNPs and HA-MNPs were determined to be 84.6 ± 32.4nm and 137 ± 53.2nm, respectively. After the conjugation of Hyaluronic acid MNPs, the size slightly increased due to the large molecular weight of Hyaluronic

acid (1000kDa). In addition, the surface charge of aminated MNPs also changed from 20.62 ± 1.96 mV(aminated water soluble MNP) to -17.76 ± 1.64 mV (HA coated MNP) due to the presence of HA (Fig. 2.).
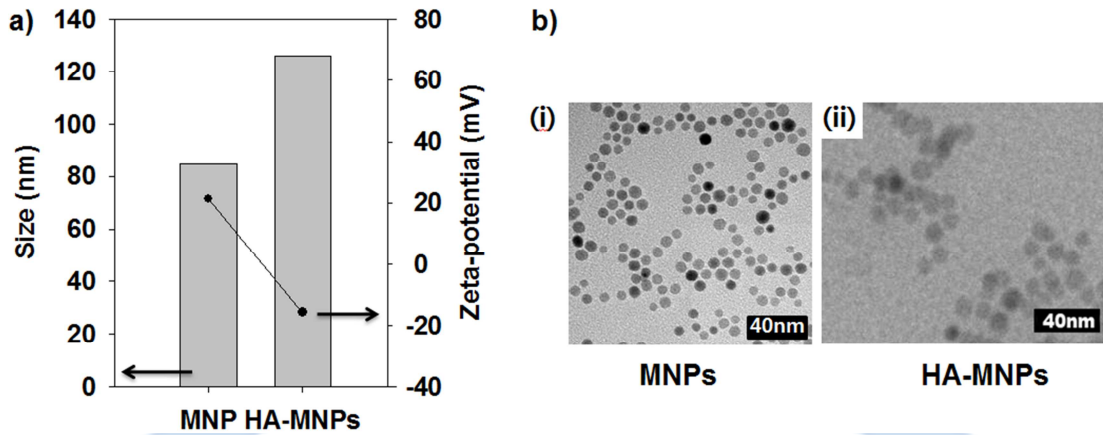
Fig.2. . (a) is The average size (gray bar) and zeta potential (black circle) and   (b) is TEM images of (i) magnetic nanoparticles (ii) hyaluronan-modified magnetic nanoparticles (HA-MNP)

2.2 Solubility and magnetic sensitivity of HA-MNPs

To assess the potential use of HA-MNPs as MR imaging agents, we performed MR imaging experiments using HA-MNPs, exhibiting the highest magnetic properties with appropriate size to avoid RES detection and prolong

retention in the circulation. In Fig. 2 (a) (i), the T2-weighted MR image exhibited a strong black color, which signified a decrease in signal intensity for the thicker HA-MNP solution. In Fig. 2 (b) (ii) represent change of intensity between of T2-weighted MR solution image
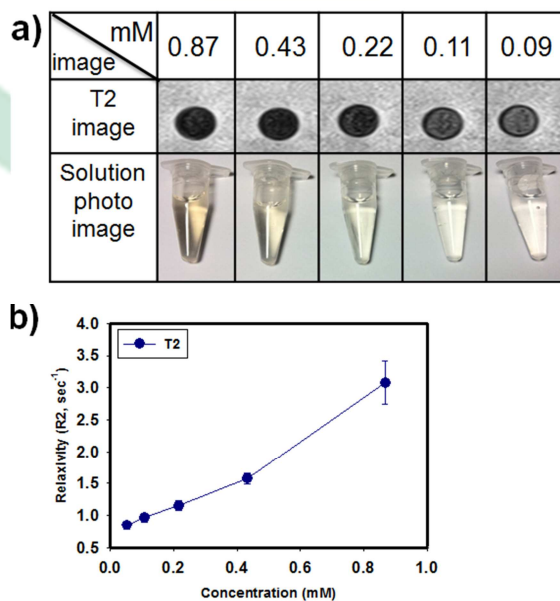
Fig.3. (a) Photographs and T2 solution MR images of HA-MNPs each conditions and (b) R2 relaxivity graph for the

magnetic ion concentration.
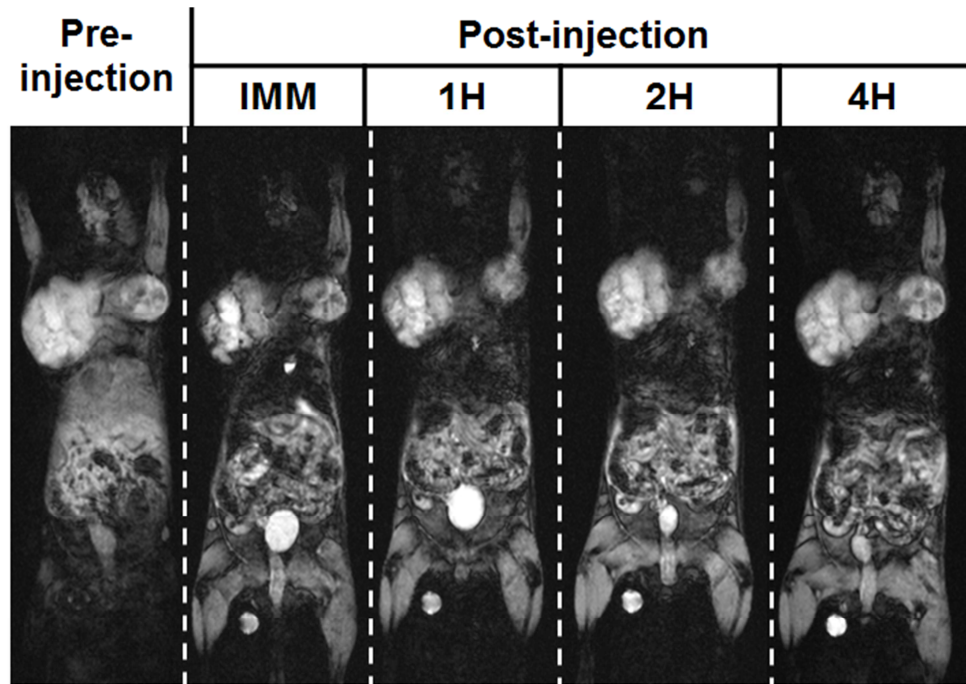
Fig.4. T2 MR images of tumor-bearing mice after intravenous injection of HA-MNPs. FOV: 100mm, ST: 1.00mm, TR: 14.85ms, TE: 5.65ms, coil elements: Wrist coil, Imaging modality: Siemens MR scanner

2.4 In vivo MR image

In Fig. 4, MR signal enhancement was identified after HA-MNPs injection. Initially, the center of tumor instantly darkened, and enhanced MR imaging signal intensity at surrounding vessels was simultaneously observed. In T2 weight MR images, clear anatomic details were observed,

3. CONCLUSION

In summary, we synthesized HA-MNPs as MR imaging agents for effective diagnosis for CD44-overexpressing breast cancer.. Further study, we plan to evaluate as a molecular imaging tool using variable MR sequence for better imaging technique.

4. EXPERIMENTAL METHOD

4.1. Materials

Polysorbate 80, ethylenediamine, 1,4-dioxane (99.8％), 4-dimethylaminopyridine, triethylamine, and succinic anhydride (SA) were purchased from Sigma Aldrich Chemical Co. Phosphate buffered saline (PBS: 10 mM, pH 7.4), Roswell Park Memorial Institute-1640 (RPMI-1640), fetal bovine serum and antibiotic-antimycotic solution were purchased from Gibco and dialysis membrane (molecular weight cut off: 1,000 Da) was obtained from Spectrum laboratory. Hyaluronic acid (HA, 1,000,000 Da) was purchased from Yuhan Phrmaceutical Corporation (Seoul, Korea). MDA-MB-231 cell lines (American Type Culture Collection) were grown in medium containing 10% fetal bovine serum and 1% Antibiotic-Antimycotic at 37℃, humidified 5% CO_2 atmosphere.

4.2. Synthesis of magnetic nanoparticles

To synthesize monodispersed magnetic nanoparticles (MNPs), 2 mmol of iron (III) acetylacetonate, 1 mmol of manganese(II) acetylacetonate, 10 mmol of 1,2-hexadecanediol, 6 mmol of dodecanoic acid, and 6 mmol of dodecylamine were dissolved in 20 mL of benzyl ether under an ambient nitrogen atmosphere. The mixture was then pre-heated to 200°C for 2 hours and refluxed at 300°C for 30 minutes. After the reactants were cooled at room temperature, the products were purified with an excess of pure ethanol. Approximately 11 nm of MNPs were synthesized using the seed-mediated growth method.

4.3. Preparation of hyaluronan-modified magnetic nanoparticles (HA-MNPs)

HA-MNPs were prepared by the nano-emulsion method. 30 mg of magnetic nanoparticle were dissolved in 4 mL hexane (organic phase). This organic phase was poured into 20 mL deionized water (aqueous phase) containing 30 mg HA. The solution was ultra-sonicated in an ice-cooled bath for 20 min at 190W and stirred overnight at room temperature to evaporate the organic solvent. The resulting suspension was centrifuged three times for 20 min each at 3000 rpm. After the supernatant was removed, the precipitated HA-MNPs were re-dispersed in 5 Ml deionized water. The size distribution and zeta potential of HA-MNPs were analyzed by laser scattering (ELS-Z, Otsuka Electronics); morphologies were confirmed using a transmittance electron microscope (TEM, JEM-2100, JEOL Ltd. Japan.). Finally, the relaxivity (R2) data of HA-MNPs solution were measured through magnetic resonance (MR) imaging analysis.

4.7. Heterotopic animal model and experimental procedure

All animal experiments were conducted with the approval of the Association for Assessment and Accreditation of Laboratory Animal Care (AAALAC) International. Female BALB/C-Slc nude mice at 7-8 weeks of age were anesthetized by intraperitoneal injection of a Zoletil/Rompun mixture and injected with 200 mL

containing. 1.0×10^7 MDA-MB-231 cells suspended in saline into the femoral region. After cancer cell implantation, MR imaging was performed between 2 and 3 weeks. After MR imaging organ MR imaging performed too. In addition, the extracted tumor tissues from tumor-bearing mice treated with HA-MNPs were frozen, sectioned, and stained using Prussian blue. All stained tissue sections were analyzed using a virtual microscope (Olympus BX51, Japan) and Olyvia software.

4.8. MR imaging

Animal, organ, solution and cell MR imaging experiments were performed with a 3 Tesla Siemens clinical MRI instrument using a wrist coil with T2 Turbo spin echo sequence. (T2 Turbo spin echo: TR: 4000ms, TE : 114ms ,Slice thickness : 1.0mm, FOV read : 180mm)

Acknowledgments

Reference

[1] Kim JK, Choi KJ, Lee M, Jo MH, Kim S. Molecular imaging of a cancer-targeting theragnostics probe using a nucleolin aptamer- and microRNA-221 molecular beacon-conjugated nanoparticle. Biomaterials 2012;33(1):207-217.

[2] Kircher MF, Hricak H, Larson SM. Molecular imaging for personalized cancer care. Molecular oncology 2012;6(2):182-195.

[3] Meng X, Loo BW, Jr., Ma L, Murphy JD, Sun X, Yu J. Molecular imaging with 11C-PD153035 PET/CT predicts survival in non-

small cell lung cancer treated with EGFR-TKI: a pilot study. Journal of nuclear medicine : official publication, Society of Nuclear Medicine 2011;52(10):1573-1579.

[4]   Gong P, Shi B, Zheng M, Wang B, Zhang P, Hu D, Gao D, Sheng Z, Zheng C, Ma Y, Cai L. PEI protected aptamer molecular probes for contrast-enhanced in vivo cancer imaging. Biomaterials 2012.

[5]   Blasberg RG. Molecular imaging and cancer. Molecular cancer therapeutics 2003;2(3):335-343.

[6]   Hoffman JM, Menkens AE. Molecular imaging in cancer: future directions and goals of the National Cancer Institute. Academic radiology 2000;7(10):905-907.

[7]   Bzyl J, Lederle W, Rix A, Grouls C, Tardy I, Pochon S, Siepmann M, Penzkofer T, Schneider M, Kiessling F, Palmowski M. Molecular and functional ultrasound imaging in differently aggressive breast cancer xenografts using two novel ultrasound contrast agents (BR55 and BR38). European radiology 2011;21(9):1988-1995.

[8]   Nishino M, Jackman DM, Hatabu H, Janne PA, Johnson BE, Van den Abbeele AD. Imaging of lung cancer in the era of molecular medicine. Academic radiology 2011;18(4):424-436.

[9]   Kiessling F. Science to practice: the dawn of molecular US imaging for clinical cancer imaging. Radiology 2010;256(2):331-333.

[10]   Pinker K, Stadlbauer A, Bogner W, Gruber S, Helbich TH. Molecular imaging of cancer: MR spectroscopy and beyond. European

journal of radiology 2012;81(3):566-577.

[11]   Artemov D, Mori N, Okollie B, Bhujwalla ZM. MR molecular imaging of the Her-2/neu receptor in breast cancer cells using targeted iron oxide nanoparticles. Magnetic resonance in medicine : official journal of the Society of Magnetic Resonance in Medicine / Society of Magnetic Resonance in Medicine 2003;49(3):403-408.

[12]   Gossmann A, Okuhata Y, Shames DM, Helbich TH, Roberts TP, Wendland MF, Huber S, Brasch RC. Prostate cancer tumor grade differentiation with dynamic contrast-enhanced MR imaging in the rat: comparison of macromolecular and small-molecular contrast media--preliminary experience. Radiology 1999;213(1):265-272.

[13]   Tan MQ, Burden-Gulley SM, Li W, Wu XM, Lindner D, Brady-Kalnay SM, Gulani V, Lu ZR. MR Molecular Imaging of Prostate Cancer with a Peptide-Targeted Contrast Agent in a Mouse Orthotopic Prostate Cancer Model. Pharmaceutical research 2012;29(4):953-960.

[14]   Pinker K, Stadlbauer A, Bogner W, Gruber S, Helbich TH. Molecular imaging of cancer: MR spectroscopy and beyond. European journal of radiology 2012;81(3):566-577.

[15]   Song HT, Suh JS. Cancer - Targeted MR Molecular Imaging. J Korean Med Assoc 2009;52(2):121-124.

[16]   Grenier N, Quesson B, de Senneville BD, Trillaud H, Couillaud F, Moonen C. Molecular Mr Imaging and Mr-Guided Ultrasound Therapies in Cancer. JBR-BTR

2009;92(1):8-12.

[17] Artemov D, Mori N, Okollie B, Bhujwalla ZM. MR molecular imaging of the Her-2/neu receptor in breast cancer cells using targeted iron oxide nanoparticles. Magnet Reson Med 2003;49(3):403-408.

[18] Gossmann A, Okuhata Y, Shames DM, Helbich TH, Roberts TPL, Wendland MF, Huber S, Brasch RC. Prostate cancer tumor grade differentiation with dynamic contrast-enhanced MR imaging in the rat: Comparison of macromolecular and small-molecular contrast media - Preliminary experience. Radiology 1999;213(1):265-272.

[19] Thomas D, Bal H, Arkles J, Horowitz J, Araujo L, Acton PD, Ferrari VA. Noninvasive assessment of myocardial viability in a small animal model: comparison of MRI, SPECT, and PET. Magnetic resonance in medicine : official journal of the Society of Magnetic Resonance in Medicine / Society of Magnetic Resonance in Medicine 2008;59(2):252-259.

[20] Coimbra A, Williams DS, Hostetler ED. The role of MRI and PET/SPECT in Alzheimer's disease. Current topics in medicinal chemistry 2006;6(6):629-647.

[21] Spencer SS, Theodore WH, Berkovic SF. Clinical applications: MRI, SPECT, and PET. Magnetic resonance imaging 1995;13(8):1119-1124.

[22] Kim AY, Han JK, Seong CK, Kim TK, Choi BI. MRI in staging advanced gastric cancer: is it useful compared with spiral CT? Journal of computer assisted tomography 2000;24(3):389-394.

[23] Portnoi LM, Denisova LB, Stashuk GA, Nefedova VO. [Magnetic resonance imaging in the diagnosis of gastric cancer: X-ray versus MRI anatomic findings]. Vestnik rentgenologii i radiologii 2000(1):26-40.

[24] Bradbury M, Hricak H. Molecular MR imaging in oncology. Magnetic resonance imaging clinics of North America 2005;13(2):225-240.

[25] Delikatny EJ, Poptani H. MR techniques for in vivo molecular and cellular imaging. Radiologic clinics of North America 2005;43(1):205-220.

[26] de Zwart IM, de Roos A. MRI for the evaluation of gastric physiology. European radiology 2010;20(11):2609-2616.

[27] Takeda M, Amano Y, Machida T, Kato S, Naito Z, Kumita S. CT, MRI, and PET findings of gastric schwannoma. Japanese journal of radiology 2012.

[28] Motohara T, Semelka RC. MRI in staging of gastric cancer. Abdominal imaging 2002;27(4):376-383.

[29] Spieth ME, Gauger BS. Time-resolved 3D MRI of gastric emptying. AJR American journal of roentgenology 2004;182(1):259; author reply 259.

[30] Das CJ, Debnath J, Mukhopadhyay S. MRI appearance of giant gastric lymphangioma. Indian journal of gastroenterology : official journal of the Indian Society of Gastroenterology 2006;25(2):81.

[31] Kim IY, Kim SW, Shin HC, Lee MS, Jeong DJ, Kim CJ, Kim YT. MRI of gastric carcinoma: results of T and N-staging in an in vitro study. World journal of gastroenterology : WJG 2009;15(32):3992-3998.

[32] Tan M, Burden-Gulley SM, Li W, Wu X, Lindner D, Brady-Kalnay SM, Gulani V, Lu ZR. MR molecular imaging of prostate cancer with a peptide-targeted contrast agent in a mouse orthotopic prostate cancer model. Pharmaceutical research 2012;29(4):953-960.

[33] Buijs M, Kamel IR, Vossen JA, Georgiades CS, Hong K, Geschwind JF. Assessment of metastatic breast cancer response to chemoembolization with contrast agent enhanced and diffusion-weighted MR imaging. Journal of vascular and interventional radiology : JVIR 2007;18(8):957-963.

[34] Rydland J, BjOrnerud A, Haugen O, Torheim G, Torres C, Kvistad KA, Haraldseth O. New intravascular contrast agent applied to dynamic contrast enhanced MR imaging of human breast cancer. Acta Radiol 2003;44(3):275-283.

[35] Nikolaou K, Kramer H, Grosse C, Clevert D, Dietrich O, Hartmann M, Chamberlin P, Assmann S, Reiser MF, Schoenberg SO. High-spatial-resolution multistation MR angiography with parallel imaging and blood pool contrast agent: initial experience. Radiology 2006;241(3):861-872.

[36] Stracke CP, Katoh M, Wiethoff AJ, Parsons EC, Spangenberg P, Spuntrup E. Molecular MRI of cerebral venous sinus thrombosis using a new fibrin-specific MR contrast agent. Stroke; a journal of cerebral circulation 2007;38(5):1476-1481.

[37] McDannold N, Fossheim SL, Rasmussen H, Martin H, Vykhodtseva N, Hynynen K. Heat-activated liposomal MR contrast agent: initial in vivo results in rabbit liver and kidney. Radiology 2004;230(3):743-752.

[38] Lim EK, Kim HO, Jang E, Park J, Lee K, Suh JS, Huh YM, Haam S. Hyaluronan-modified magnetic nanoclusters for detection of CD44-overexpressing breast cancer by MR imaging. Biomaterials 2011;32(31):7941-7950.

[39] He Y, Wu GD, Sadahiro T, Noh SI, Wang H, Talavera D, Vierling JM, Klein AS. Interaction of CD44 and hyaluronic acid enhances biliary epithelial proliferation in cholestatic livers. American journal of physiology Gastrointestinal and liver physiology 2008;295(2):G305-312.

[40] Knupfer MM, Poppenborg H, Hotfilder M, Kuhnel K, Wolff JE, Domula M. CD44 expression and hyaluronic acid binding of malignant glioma cells. Clinical & experimental metastasis 1999;17(1):71-76.

[41] Miyake H, Hara I, Okamoto I, Gohji K, Yamanaka K, Arakawa S, Saya H, Kamidono S. Interaction between CD44 and hyaluronic acid regulates human prostate cancer development. The Journal of urology 1998;160(4):1562-1566.

[42] Lesley J, Hyman R. CD44 can be activated to function as an hyaluronic acid receptor in normal murine T cells. European journal of immunology 1992;22(10):2719-2723.

[43] Hyman R, Lesley J, Schulte R. Somatic cell

mutants distinguish CD44 expression and hyaluronic acid binding. Immunogenetics 1991;33(5-6):392-395.

[44]   Zhang W, Gao L, Qi S, Liu D, Xu D, Peng J,

Daloze P, Chen H, Buelow R. Blocking of CD44-hyaluronic acid interaction prolongs rat allograft survival. Transplantation 2000;69(4):665-667.

Ethics in Publication

Article reprints from ScholarGen Publishers commit to promote your research work with its professional quality reprints service delivered directly to your door at an affordable value. It aims to display the potential of the article at interviews, conferences, distribution to colleagues, seminars and other promotional activities. Reprints are produced from the final PDF of the article.

As all articles are open access, readers are free to download and/or print copies from the website, according to the terms & conditions of the ScholarGen Publishers License . Authors must agree to distribute such reprints without any alterations, additions, deletions, overprinting, highlighting, promotional messages, or promotional attachments.

Author Reprints : Author reprints are solely for the author's personal, noncommercial use. Author reprints are available in both B/W and color format with the addition of a standard cover page. Each article reprint is available with cover pages of the journal itself in order to maximum the impact and highlight the prestige of the content.

The front cover of the Reprints consists of :

- Publisher logo
- Name/logo of the journal
- Title of article, complete list of authors, and Article information

Commercial Reprints : Commercial reprints are high quality with specially designed covers. The reprints are an exact replica of the published article. These reprints are available only in the color format with the customized cover page.

Ethical Principles: Authors are expected to stick to the ethical standards and conduct that remain mandatory in scholarly publishing. During the submission, authors need to mention that their work has not been submitted elsewhere, instances (if any) & conflicts need to be stated and plagiarism must be strictly cross checked. For Animal/ Human models, ethical authorization copy needs to be submitted.

Breach of copyright/ Plagiarism: Plagiarism can be defined as making a replica of the published content. ScholarGen Publishers strictly against the Plagiarism. We cross check every submission that is been submitted to any of its peer reviewed Journal. Any submission that has partially /completely plagiarized content will be rejected immediately after submission.

Attribution Practice: Citations need to be acknowledged for previously published content. It is obligatory when new ideas or results are produced. If the author fails to reproduce citation for any previous work, it will be considered as technical plagiarism and the paper might be rejected immediately.

Conflicts of Interest: ScholarGen Publishers involves double blind peer review system to avoid conflicts for the submitted manuscript. The authors should hold responsibility in providing conflicts if any to avoid further conflicts.

Confidentiality Protection: Editors, Reviewers need to be very cautious while handling the research work of the authors. It is ethically not accepted to use/disseminate the unpublished work. Use of the unpublished work might consider for legal actions.

Human and Animal Rights: Clear statements of ethical clearance documents need to be provided if applicable. The work involving animal models and human volunteers need to submit the essential statements.

Consents/Instances: Author needs to state consents and instances if any to avoid further obligations. Clear statement with written signature must be presented by the author while submitting his/her work.

Civility & Misconduct Allegations: Editors, Reviewers, Authors & the Journal staff are expected to adhere to the basic professional courtesy. Any verbal abuse, debates and insult is highly offended by the ScholarGen Publishers. The supposed misconducts are severely offended further.

Scholargen Journal of Medical Imaging

Volume 01 Number 01 September 2018